NUMERICAL ANALYSIS FOR FILM COOLING PERFORMANCE UNDER DIFFERENT JET DESIGN CRITERIA

by

Mohammed Aref Al-Hemyari

A Thesis presented to the Faculty of the
American University of Sharjah
College of Engineering
In Partial Fulfillment
of the Requirements
for the Degree of

Master of Science in
Mechanical Engineering

Sharjah, United Arab Emirates

April 2018

Approval Signatures

We, the undersigned, approve the Master's Thesis Mohammed Aref Al-Hemyari

Thesis Title: Numerical Analysis for Film Cooling Performance Under Different Jet Design Criteria

Signature	**Date of Signature** (dd/mm/yyyy)
_____	_____
Dr. Mohammad Omar Hamdan Associate Professor, Department of Mechanical Engineering Thesis Advisor	
_____	_____
Dr. Mehmet Fatih Orhan Associate Professor, Department of Mechanical Engineering Thesis Co-Advisor	
_____	_____
Dr. Imran Qureshi Assistant Professor, Department of Mechanical Engineering Thesis Committee Member	
_____	_____
Dr. Rachid Chebbi Professor, Department of Chemical Engineering Thesis Committee Member	
_____	_____
Dr. Mamoun Abdel-Hafez Head, Department of Mechanical Engineering	
_____	_____
Dr. Ghaleb Husseini Associate Dean for Graduate Affairs and Research College of Engineering	
_____	_____
Dr. Richard Schoephoerster Dean, College of Engineering	
_____	_____
Dr. Mohamed El-Tarhuni Vice Provost for Graduate Studies	

Acknowledgement

I would like to express gratitude to my advisor, Dr. Mohammad O. Hamdan, for his patience, guidance and wise mentoring throughout all stages of this work. I would like as well to give my appreciation to my co-advisor, Dr. Mehmet Fatih Orhan and my thesis committee Dr. Imran Qureshi and Dr. Rachid Chebbi for investing time and effort to improve the thesis.

I would also like to thank Dr. Abdul Hai Al-Alami for his continuous support in my whole academic life. Finally, I would like to thank the Department of Mechanical Engineering at the American University of Sharjah and Graduate Teaching Assistants GTA in college of engineering for sponsoring me in my master's degree. To my fellow colleagues

Dedication

To my father Aref, who supported me in all stages in life. He who made sure that I only focus on future and used every possible opportunity to support and guide me by all means. To my Mother Altaf, for her patience love and compassion. For my wife Reinad, for her continuous support and unconditional love. For my family and friends. This work is dedicated to you, Thank you for all the support.

Abstract

Cooling gas turbine blades is a crucial technique to allow higher turbine inlet temperatures. A higher turbine inlet temperature allows boosting gas turbine efficiency, which reduces fuel consumption. One of the main cooling techniques of the turbine blades is film cooling where a relatively low air temperature is used to form a blanket of cool air around the blade to shield it from high temperature gases. Many complex interrelated geometry and flow parameters affect the effectiveness of the film cooling. The complex interrelations between these parameters are considered the main challenge in properly understanding the effect of these parameters on film cooling. Testing such cooling techniques under actual engine conditions is even more challenging due to difficulty of installing proper instrumentations. Numerical techniques are viable analysis techniques that are used to better understand film cooling techniques. In this study, a simplified 2D film cooling jet blown from the slot jet is investigated under multiple variable parameters, mainly, the blowing ratio, jet angle, density ratio and centrifugal force. The performance of the film cooling is reported using local and average adiabatic film effectiveness. The main contribution of this study is exploring the effect of the centrifugal force and wall material selection using conjugate heat transfer on film cooling effectiveness. The centrifugal force reduces the overall adiabatic film effectiveness. A correlation between the blowing ratio, density ratio and injection angle is developed in this work. The highest film cooling performance was founded at a blowing ratio of 0.8, an injection angle of 30° and density ratio of 1.2.

Keywords: ***Film-cooling; film effectiveness; conjugate heat transfer; centrifugal force; CFD.***

Table of Contents

List of Figures

List of Tables

List of Abbreviations

2D	Two-dimensional
a_c	Centripetal acceleration, $[\frac{m}{s^2}]$
AFCE	Adiabatic Film Cooling Effectiveness
C_p	Specific heat, $[J/kg.K]$
D	Slot diameter, $[m]$
DR	Density ratio of coolant to mainstream gas, [-]
EWF	Enhanced wall function
F	Centrifugal force
FCE	Film cooling effectiveness
I	Turbulence intensity, $[I = \frac{\acute{u}}{V_h}]$
K_R	Thermal conductivity ratio, [-]
k	Turbulence kinetic energy, $[m^2/s^2]$
k_c	Thermal conductivity, $[\frac{W}{m.K}]$
L	Mainstream entrances length, $[m\ ]$
M	Blowing ratio, [-]
P	Pressure, [kPa]
Pr	Prandtl number, [-]
RSM	Response surface method
RNG	Reynolds normalization group
RPM	Revolution per minutes
SST	Menter's shear stress transport
T	Temperature, $[K]$

u_τ	Friction velocity $[m/s]$
V	Velocity, $[m/s]$
VR	Velocity ratio of coolant to mainstream gas, [-]
x	Distance in the mainstream gas flow direction, $[m]$
y	Distance in the hole normal direction, $[m]$
y^+	Dimensionless wall unit, [-]

Greek symbols

α	Injection angle. [deg]
ε	Turbulence dissipation rate, $[\frac{J}{kg.s}]$
η	Film cooling effectiveness, [-]
μ	Dynamic viscosity, $[\frac{kg}{m.s}]$
ρ	Density, $[\frac{kg}{m^3}]$
τ_w	Wall shear stress, $[Pa]$
ω	Turbulence specific dissipation rate, $[1/s]$

Subscripts

ad	Adiabatic
av	Average
c	Coolant jet
h	Mainstream gas
w	Wall
t	Turbulent

Chapter 1. Introduction

In this chapter, a short introduction is provided about different cooling techniques used in gas turbine engines. Then, a description of the investigated problem is presented with the main thesis contribution. Finally, a general organization of the thesis is presented.

1.1. Overview

Gas turbine engines are considered an integral vital part of the energy map of today's world. They are used in aircraft, cars, marine applications and power generation. Gas turbine's power output and thermal efficiency increases with the increase of turbine's inlet temperature [1]. Advanced gas turbine engines operate at temperatures higher than 1,200 ℃ [2, 3]. This temperature causes hot spot formation and increased wall thermal stresses on turbine's blade which reduces the turbine blade life. To assure realistic turbine blade life, the variation on the blade wall temperature must be limited [4]. Remarkable work has been done in the field of material science and cooling techniques to increase the turbine maximum allowed inlet gas temperature while achieving realistic durability goals. Since the introduction of aircraft gas turbine in 1941, the average rate of increasing the maximum allowable inlet temperature using cooling techniques is around 20℃/year which is more than double the rate achieved by material scientist [5]. Most of today's advanced gas turbines utilizes cooling techniques in their gas turbine blade. Cooling techniques are classified into internal cooling methods such as internal jet impingement [6-10] and external methods such as transpiration cooling [11, 12] and film cooling [13, 14]. Most of the modern gas turbine utilizes film cooling technique as the primary cooling technique in gas turbine engines as it allows higher inlet temperatures and relatively has lower fabrication and maintenance costs [15].

Figure 1 shows a schematic of a turbine blade adapting film cooling technique. The coordinates represent the flow freestream direction, x and the direction normal to the hole in zone 1, y.

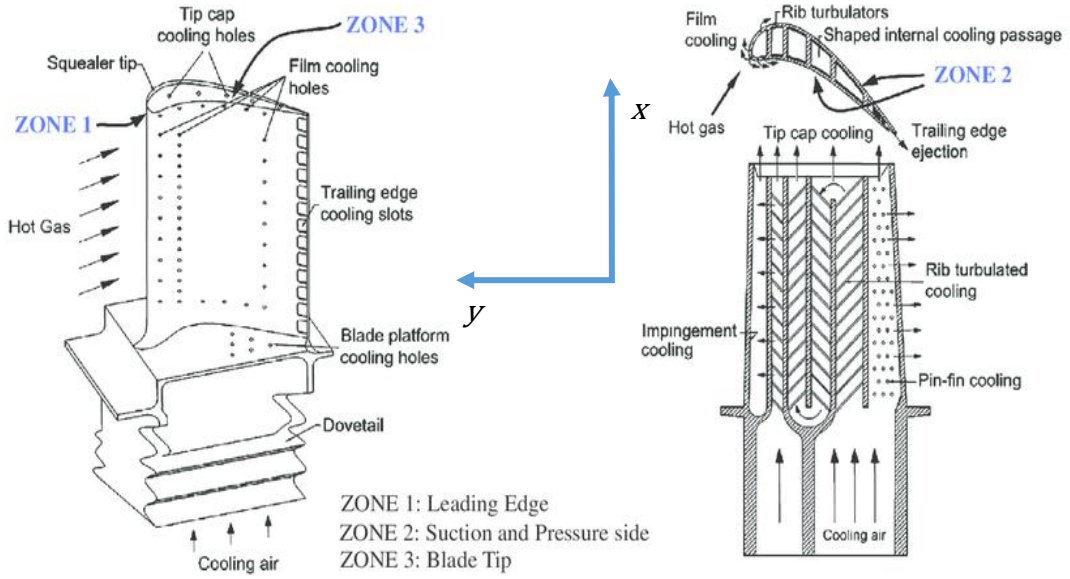

Figure 1: A cooled turbine blade configuration, illustrating the complex interaction between internal and external flows [3]

In film cooling technique, a relatively low temperature bleed air is taken from the compressor to flow through small holes over the turbine blade surface forming a protective layer on the turbine blade separating the blade from the hot mainstream gas [13]. This protective film layers reduces the heat transfer significantly between the hot mainstream gas and the turbine blade surface which allows higher mainstream gas temperature to enter the turbine without negatively affecting the turbine durability [14]. The film cooling performance is reported using film cooling effectiveness (FCE) which is defined as follow:

$$\eta = \frac{T_h - T_w}{T_h - T_c} \qquad (1)$$

where η is the film cooling effectiveness, T_h is the mainstream gas temperature, T_w is the turbine's blade wall temperature and T_c is the coolant gas temperature.

Modern gas turbine blades often fabricated from nickel-based superalloys due to its high melting point and relatively low thermal conductivity [16]. In most of the cases turbine blade wall can be approximated as an adiabatic wall and hence Equation 1 transforms to Equation 2. Hence, η_{ad} is known as adiabatic film cooling effectiveness (AFCE). Both parameters, FCE and AFCE, are commonly used in literature.

$$\eta_{ad} = \frac{T_h - T_{ad,w}}{T_h - T_c} \tag{2a}$$

where $T_{ad,w}$ is the turbine's blade adiabatic wall temperature.

Another parameter that is used in literature is averaged AFCE which represents the area average for AFCE calculated over unit area. The averaged AFCE is mathematical represented as follow:

$$\eta_{avg,ad} = \frac{1}{A}\int \eta_{ad}\ dA \tag{2b}$$

For 2D dimensional problem consider in this study the above Equation is calculated with unit of depth of one as follow:

$$\eta_{avg,ad} = \frac{1}{L}\int \eta_{ad}\ dx \tag{2c}$$

1.2. Thesis Objectives

The main objective of the thesis is to develop a two-dimensional (2D) numerical model that will be used to evaluate film cooling performance at different geometrical and flow parameters using the commercial software ANSYS FLUENT. A parametric study is carried in this study that reports the significance of the main parameters affecting the AFCE using response surface methodology. These main parameters affecting the AFCE are blowing ratio (*M*), injection angle (α) and density ratio (*DR*). Response surface methodology (RSM) is used to describe the single contribution of the different studied parameters on the AFCE. This study addresses the effect of centrifugal force on the AFCE on the span-wise direction of a turbine blade. Also, the study explores the effect of different blade material on the coolant chamber and how this can eventually affect the AFCE of the turbine blade.

1.3. Research Contribution

The main outcomes of this thesis are as follows:

1. A 2D numerical model that can be used to estimate the AFCE under different geometrical and flow parameters. This will be used to find the best combinations of these parameters that offers the highest AFCE.
2. Sensitivity analysis of the main parameters affecting the AFCE of the 2D numerical model. The sensitivity study is used to report the significance of every factor and to generate a model that estimates the AFCE at a wide range of the chosen parameters.

3. Study the effect of jet Reynolds number on AFCE.
4. Study the effect of centrifugal force on the AFCE at the tip cooling holes.
5. Study the effect of blade thermal conductivity. Different blade materials with variable thermal conductivity is investigated to explore its impact on the FCE.

1.4. Thesis Organization

The rest of the thesis is organized as follows: Chapter 2 provides background about film cooling and recent development and modelling techniques. The employed numerical method is discussed in Chapter 3 along with the problem schematic and boundary conditions. Chapter 4 presents the results of the numerical study with discussion of the numerical results such as AFCE. Finally, Chapter 5 concludes the thesis and outlines the future work.

Chapter 2. Background and Literature Review

In this chapter, a literature survey related to the turbine film cooling techniques is introduced. At first, a comprehensive review of the main parameters affecting the AFCE has been reported. Then, a review for the impact of centrifugal forces and conjugate heat transfer on film cooling is presented. Finally, a review of recent numerical publications, that handle numerical simulation of film cooling, are presented.

2.1. Main Parameters Affecting the Performance of Film Cooling

A very wide list of parameters that affect the performance of the film cooling were reported in literature. Researchers have experimentally and numerically investigated the performance of film cooling parameters.

The main parameters the AFCE can be classified into two main classifications; flow parameters and geometrical parameters. Flow parameters are generally reported in terms of blowing ratio (M), density ratio (DR) and turbulence intensity (I) while geometrical parameters are reported in terms of injection angle (α), hole shape, number of holes, jet delivery channel length and hole to hole spacing. All these parameters are interrelated, and their combinations affect the performance of the adiabatic film effectiveness.

2.1.1 Flow parameters

The first most widely reported flow parameter that affects AFCE is the blowing ratio. Blowing ratio represents the ratio of velocity and density of coolant flow to mainstream flow. The relatively cool air that is used to form a protective blanket around the airfoil is called the coolant flow or jet flow. The hot gas running over the blade is known as the mainstream flow. Equation (3a) shows the mathematical representation of the blowing ratio.

$$M = \frac{\rho_c V_c}{\rho_h V_h} \tag{3a}$$

where M is the blowing ratio, ρ_c is the density of the coolant gas, V_c is the velocity of the coolant gas, ρ_h is the density of the mainstream gas and V_h is the velocity of the mainstream gas.

A numerical study by Nijo et al. [17], showed that as the blowing ratio increases to 1.5 the adiabatic film cooling effectiveness increases. However, operating at blowing ratios above 2 reduces the adiabatic film cooling effectiveness directly after the hole and increasing it at distances greater than $x/D = 8$. This has been explained by the detachment of coolant film from the surface, which causes of wakes and vortices formation within the film cooling boundary layer [18]. Plesniak and Cusano [19] presented a flow regime map to describe the relation between the blowing ratio, injection angle and the development length of the film cooling. They showed [19] that for any injection angle, increasing the blowing ratio will always increase jet penetration to the mainstream flow [19]. This will change the behavior of the coolant jet from a wall attached jet to a free jet, which reduces AFCE significantly. The same conclusion can be also found in the experimental work of Yuen and Martinez-Botas [20], where they have studied a wide range of both injection angles and blowing ratios at a low turbulence intensity (1.7%). They reported that for every injection angle there is a specific blowing ratio at which separation of coolant jet occurs. Mayhew et al. [21], have explored the effect of turbulence intensity on the previous studies. Mayhew et al. [21] has found that low turbulence intensity experiments agreed with the previous results. However, at same blowing ratio, Mayhew et al. [21] reported that high turbulence intensities (more than10%), required higher injection angle is needed to cause detachment of coolant fluid. This result was also confirmed independently by the experimental work of Mouzon et al. [22]. To conclude, the main outcome from the previous studies is that for a specific turbulent intensity value at a specific angle increasing the blowing ratio will increase the film effectiveness up to a critical blowing ratio. When this critical value is reached, the coolant jet will fail to stay attached to the plate surface and will penetrate to the mainstream causing the film cooling effectiveness to fall drastically. Increasing the turbulent intensity will increase the tendency of the coolant jet to stay attached to the plate surface, which allows the use of a higher blowing ratio. This leads to better shielding of the blade from the hot mainstream which means higher value of film cooling effectiveness.

Blowing ratio is also be expressed as follows:

$$M = \frac{\rho_c V_c}{\rho_h V_h} = DR * VR \tag{3b}$$

where DR is the density ratio, $DR = \frac{\rho_c}{\rho_h}$ and VR is the velocity ratio, $VR = \frac{V_c}{V_h}$.

The density ratio, the ratio between the coolant jet and the mainstream gas density, allows us to study the effect of jet coolant to mainstream fluid temperatures by the means of fixing the blowing ratio and varying the velocity ratio. Experimental work has shown that at a fixed blowing ratio, increasing the density ratio will increase the wall area averaged AFCE in the range of DR between 0.97 and 1.53 [23]. This is mainly due to the decrease of velocity ratio, which gives the jet relatively lower momentum to escape the plate surface. Singh et al. [24] has numerically studied the effect of density ratio on a very wide range from 1 to 12 DR. For all of the cases there was a critical density ratio at which increasing the DR beyond this value reduces the span-wise area averaged AFCE. They reported that as the injection angle increases, for a fixed blowing ratio, the critical density ratio decreases. However, as the blowing ratio increases, for a specific injection angle, the critical density ratio increases. Gas turbines operational regions are at DR values between 1 and 3, blowing ratios less than 3, and an injection angle lower than 45° [20-26]. In this specified region, the overall trend is that as the DR increases the averaged AFCE decreases. Finally, fixing the velocity ratio and increasing the mainstream and coolant velocity to achieve higher values of Reynolds number are studied experimentally [27- 29] and numerically [24]. It has been found that for all the blowing ratios at different flow configurations, as the Reynolds number increases, the film cooling effectiveness increases. This trend between Reynolds number and FCE is due to the fact that as Reynolds number increases, the film cooling layer will have higher momentum which causes the flow to stay attached to the plate surface.

2.1.2 Geometrical parameters

Multiple geometrical parameters affect the AFCE; namely film injection angle (α), hole shape, number of holes, jet delivery channel length and hole to hole spacing. Jia et al. [30] carried out a very extensive experimental and numerical work for angles ranging between 16°and 90°and a wide range of blowing ratio ranging between 0.5 and 9. They concluded that at the different values of blowing ratios, an injection angle of 30°achieves the highest FCE. The same conclusion has been also found at low blowing ratios range [25] and at different ratio of transverse pitch to injection angle.

Hole geometry has been investigated widely in literature with configurations ranging from the traditional cylindrical hole to complex geometries that focuses on enhancing the cooling effectiveness. Expanded holes have shown superiority compared to cylindrical holes in terms of FCE mainly due to the reduced coolant jet momentum, which causes the jet to stay attached to walls. This type of hole have been first reported by Goldstein et al. [31] A comparison between cylindrical holes and expanded holes has been reported by Thole et al. [32] where they showed that the effectiveness have significantly increased relative to cylindrical hole due to lower jet penetration capabilities and lower intense shear region. A compounded angle hole, which is a cylindrical hole with an expanded exit by an angle of 60°, have been compared to a cylindrical hole by Schmidt et al. [33]. It has been reported that compound angle hole offered a higher effectiveness at higher momentum ratios and similar effectiveness at lower momentum ratios. Novel shaped holes have been also reported by Dai and Lin [34] who numerically studied film cooling effectiveness for shaped and crescent holes. Complex structures such as double-jet holes [35], trenched holes [36] and hybrid scheme holes [37] were also proven to improve FCE. Converging slot holes were compared to cylindrical holes by Yao et al. [38]. They [38] have experimentally investigated the effect of the two-hole configuration on the FCE and on the heat transfer coefficient. It was reported [38] that converging holes offers higher FCE and heat transfer coefficient.

These different hole geometry studies focus mainly on controlling the formation of the film layer around the turbine blade by the means of increasing the coverage area of the film cooling and by reducing the chances of the coolant jet to detach the turbine blade wall.

In this study, a numerical simulation is used to study slot-hole configuration using a 2D model. There are four main advantages of using slot shaped jet in analyzing film-cooling effect. First, it reduces number of geometrical parameters and magnifies the impact of the jet angle. Second, this assumption reduces the problem size since 2D mesh require less computation time. Third, it allows reducing the impact of geometrical parameters on other important parameters such as blowing ratio, density ratio, etc. Finally, it is much easier to experimentally validate such geometry, which explain the availability of such published experimental work.

Therefore, in this study the focus will be in the following parameters:

1. Blowing ratio
2. Density Ratio
3. Injection angle
4. Jet Reynolds number
5. Centrifugal force
6. Thermal conductivity ratio between solid and fluid

2.2. Centrifugal Force

Few studies available in literature that have explored the impact of centrifugal force on film cooling. The experimental difficulty has limited number of these studies. The impact of centrifugal force on film cooling effectiveness is expected since centrifugal force will act as body force that would alter the flow direction and could impact the film attachment to the wall. The magnitude of the centrifugal force is directly related to engine angular speed, which often operates around 1000 RPM. Zhu et al. [39] experimentally and numerically reported the performance of FCE at low angular speed conditions. For a rotor with 300 RPM, their results have showed that the centrifugal force effects on the pressure side of the turbine blade are more significant than on the suction side. Zhu et al. [39] has reported that the span-wise area averaged FCE drops as flow moves towards the blade tip. Alzurfi et al. [40] numerically studied the effect of centrifugal force on a low speed 1-1/2 turbine stages. Alzurfi et al. [40] reported that the low FCE at the pressure side is mainly due to a favorable pressure driving the coolant away from the blade wall, while an adverse pressure gradient is observed at the suction side forcing the coolant to stay attached to the wall. These different pressure gradients have caused flow detachment and attachment, which occurred at different blowing ratio and centrifugal effects on both sides. In this work, the impact of centrifugal force is explored at the blade tip cooling holes where the impact of centrifugal force is introduced using radial centripetal acceleration. This will allow studying the flow behavior for the coolant film at the blade tip cooling holes under the centrifugal force at different rotor speeds.

2.3. Conjugate Heat Transfer Effect

Numerical studies often report the effectiveness as of film cooling as AFCE, this is because most of the turbine blades are made from a low conductivity material or superalloy. To incorporate the effect of the wall thermal conductivity, conjugate heat transfer is used. Conjugate heat transfer is a term used in the literature to describe the combining effect of the heat transfer in the fluid domain and the heat transfer in the solid domains. In fluids, convection dominates the heat transfer. While in solids, conduction is the dominant parameter. The first fluid layer near the wall is stagnant due to the no-slip condition. This will enable the first fluid layer to interact with the very first solid layer by conduction. Therefore, temperature field and heat fluxes at the fluid-solid interface are continuous. Rigby and Lepicovsky [41] studied the capability of conjugate heat transfer to capture flow and heat fields of an internally cooled configuration. They reported that the numerical results implementing the conjugate heat transfer have successfully captured the experimentally obtained flow and heat fields. Silieti et al. [42] reported that different turbulence models, mainly Reynolds normalization group (RNG) $k-\varepsilon$, the realizable $k-\varepsilon$ and the Reynolds transport turbulence models, can be used to numerically capture the conjugate heat transfer effect. They reported that blade walls made from steel show a 10% deficiency in FCE compared to the AFCE. In this work, the conjugate heat transfer is used to report how much the FCE drops when materials with different thermal conductivity are in use.

2.4. Numerical Techniques Developments

Numerical work on film cooling technique is mostly focused on selecting the best turbulence model to effectively estimate film-cooling performance. Most of the published work employs Reynolds-Averaged Navier-Stokes Equations in predicting film-cooling performance. Flat-plate configuration is a very efficient approximation to investigate the effect of different flow and geometrical parameters on film cooling performance. A very challenging task is to successfully be able to model film cooling boundary layer to be able to have a consistent and accurate approximation of the heat transfer close to the wall and to be able to predict film cooling efficiency. Ferguson et al. [43] investigated the Standard $k-\epsilon$ and Reynold stress models with standard wall formulation, non-equilibrium wall modelling with two-layer wall treatment, and the RNG $k-\epsilon$ with standard wall function. They reported that the Standard $k-\epsilon$ with the two-layer wall treatment have showed the most accurate approximation of film cooling

performance in comparison to the other combinations. Later work by York and Leylek [44] showed that RNG $k-\epsilon$ with two layers wall treatment have successfully predicated the production of turbulent kinetic energy which leads to a good agreement between experimental and numerical reported film cooling effectiveness. RNG $k-\epsilon$ with the two layers wall treatment has been proven to show a good agreement with experimental data under different conditions and geometries by many researchers. [24, 25, 45].

Chapter 3. Numerical Modelling

In the present work, the film cooling techniques is studied using the commercial software ANSYS FLUENT. A 2D flat plate and slot configuration are used to study the film cooling performance. A flat plate configuration is general and simple and can be transformed to more complicated geometry using conformal mapping techniques. The use of 3D numerical analysis requires more computing power and adds more complex meshing techniques to capture how film is impinged to the mainstream flow. The use of the 2D flat plate geometry results in a more stable simulation, which is important to study the effect of the different parameters solely without the effect of the turbines blade geometry. The schematic of the investigated geometry is shown in Figure 2.

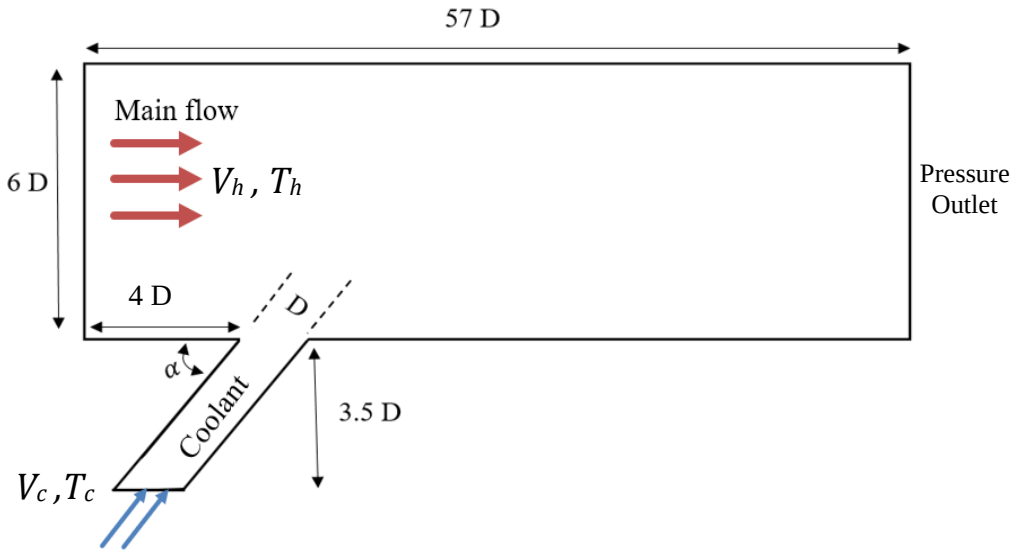

Figure 2: A schematic of the numerical model

Two flow inlets are used with one outlet. The mainstream fluid flows from the left side and is marked with red arrows as shown in Figure 2. The coolant fluid enters from the bottom plate and is marked with blue arrow with angle (α) showing the film jet direction. The slot width is D, 40 mm. The slot is located $4D$ from the downstream of the hot gas inlet, the coolant channel height is $3.5D$, the mainstream inlet height, L, is 6D and the size of the computational domain is $6D \times 57D$. The outlet is the far end of the mainstream flow direction (located at the right side of Figure 2). The dimensions are selected based on the experimental work of O'Malley [27]. All the walls are set to nonslip and adiabatic walls. In this study, in addition to the turbulence models discussed

in Section 2.4, the $k-\omega$ and the Menter's Shear Stress Transport (SST) are tested in this study to evaluate the appropriateness of these turbulence models for the 2D flat configuration case. For all $k-\epsilon$ turbulence models enhanced wall function (EWF) treatment is used for near-wall modelling. However, for $k-\omega$ and SST models near modelling is not needed as they are used in the near-wall region. The outlet boundary is treated as pressure outlet with zero-gauge pressure.

3.1. Problem Formulation

In this study, the flow is 2D, steady and incompressible. Using Reynolds-average Navier-Stokes (RANS) Equations, the governing Equations representing the studied case are mass, momentum and energy balances, which are shown below in index notation:

$$\frac{\partial(\rho u_i)}{\partial x_i} = 0 \tag{4}$$

$$\frac{\partial(\rho u_j u_i)}{\partial x_j} = -\frac{\partial P}{\partial x_j} + \frac{\partial}{\partial x_j}\left[\mu\left(\frac{\partial u_i}{\partial x_j} + \frac{\partial u_j}{\partial x_i}\right) - \rho\overline{\acute{u}_\iota \acute{u}_J}\right] \tag{5}$$

$$\frac{\partial(\rho u_j T)}{\partial x_j} = \frac{\partial}{\partial x_j}\left[\frac{\mu}{Pr}\left(\frac{\partial T}{\partial x_j}\right) - \rho\overline{\acute{T}_\iota \acute{u}_J}\right] \tag{6}$$

where u_i is the mean velocity, T is the temperature and P is pressure. The acute represent the fluctuations in the flow variable. The time averaged component in the momentum and energy Equations are called the Reynolds stress terms and are modelled using the Boussinesq hypothesis and the simple eddy diffusivity model as shown in the following Equations respectively:

$$\rho\overline{\acute{u}_\iota \acute{u}_J} = \mu_t\left(\frac{\partial u_i}{\partial x_j} + \frac{\partial u_j}{\partial x_i}\right) - \frac{2}{3}\rho k \delta_{ij} \tag{7}$$

$$\rho\overline{\acute{T}_\iota \acute{u}_J} = -\frac{\mu_t}{Pr_t}\left(\frac{\partial T}{\partial x_j}\right) \tag{8}$$

where μ_t is the turbulent viscosity, k is the turbulent kinetic energy and Pr_t is the turbulent Prandtl number. Turbulence models are used to solve Equations (4), (5) and (6) by estimating the different turbulent parameters that appear in Equations (7) and (8).

In this work, the governing Equations are discretized using the second-order upwind scheme and the pressure-velocity coupling is resolved using the semi implicit method for pressure linked Equations corrected (SIMPLEC). Solution convergence is realized when the temperature residual is lower than 10^{-9} and the velocities and continuity residuals are lower than 10^{-6}.

3.2. Air Properties

Air is the working fluid for the mainstream and coolant jet. Air is treated as an incompressible gas therefore, density is calculated using the ideal gas law. Air specific heat capacity, thermal conductivity and dynamic viscosity are obtained by Equations (9), (10) and (11) [46] where T is the temperature in kelvin.

Specific heat, C_p $(J/kg \cdot K)$:

$$C_p = 9.0813 * 10^{-11}\mathrm{T}^4 - 4.8066 * 10^{-7}\mathrm{T}^3 + 8.0735 * 10^{-4}\mathrm{T}^2 - 0.32136\mathrm{T} + 1.045 * 10^3 \quad (9)$$

Thermal conductivity, k_c $(W/m \cdot K)$:

$$k_c = 7.995 * 10^{-12}\mathrm{T}^3 - 2.4013 * 10^{-8}\mathrm{T}^2 + 8.3047 * 10^{-5}\mathrm{T} + 2.8822 * 10^{-3} \quad (10)$$

Dynamic viscosity, μ($kg/m \cdot s$) :

$$\mu = 1.7020 * 10^{-14}\mathrm{T}^3 - 4.0405 * 10^{-11}\mathrm{T}^2 + 6.8539 * 10^{-8}\mathrm{T} + 1.0616 * 10^{-6} \quad (11)$$

3.3. Turbulence Models

Different turbulence models are currently used by engineers since direct numerical simulation (DNS) is considered an expensive approach to solve the Naiver-Stokes (NS) Equations. DNS can be done by solving the time-dependent NS Equations while resolving all the scale (eddies) for a sufficient time interval so that the fluid properties reach a statistical equilibrium. DNS is possible but only for low Reynolds number flows (and simple geometries) but it is very expensive and computation time

power demanding. Time averaged quantities are appropriate and provide a more realistic approach that can be used for engineering problems such as film cooling effectiveness.

Hence, this study uses Reynolds-average Navier-Stokes (RANS) Equations which are time-averaged developed due to limitations on the computational power available in today's CPU. This will filter out most of the of the turbulence structure in the problem. This averaging leads to the appearance of unknown terms in the RANS Equations ($\rho\overline{\acute{u}_\iota\acute{u}_j}$). The turbulence models are used to accurately predict the unknown terms to solve the RANS Equations. The selection of the appropriate turbulence model is crucial in determining the quality of the solution. Different alternatives for the RANS Equations are introduced in the literature such as Scale-Resolving Simulation (SRS) model and Large Eddy Simulation (LES) model. However, they are substantially more computationally expensive than the RANS models.

The RANS models considered in this study are standard such as the Reynolds Normalization Group (RNG) $k-\varepsilon$ model, standard and SST k-ω model and the SST turbulence model. In the next section, the main details of these models are discussed [47].

3.3.1 Standard $k-\varepsilon$ model

The two-Equation standard $k-\varepsilon$ turbulence model determines both turbulent length and time scale by solving the two separate transport Equations (turbulence kinetic energy, $k=\frac{1}{2}\overline{\acute{u}_\iota\acute{u}_\iota}$, and rate of dissipation, ε). In the derivation of this model the based assumptions are that the flow is fully turbulent, and the effect of molecular viscosity is negligible. The following transport Equations are used for the two-transport Equations:

$$\frac{\partial}{\partial t}(\rho k)+\frac{\partial}{\partial x_i}(\rho k u_i)=\frac{\partial}{\partial x_j}\left[\left(\mu+\frac{\mu_t}{\sigma_k}\right)+\frac{\partial k}{\partial x_j}\right]+G_k+G_b-\rho\varepsilon-Y_M+S_k \tag{12}$$

$$\frac{\partial}{\partial t}(\rho\varepsilon)+\frac{\partial}{\partial x_i}(\rho\varepsilon u_i) =\frac{\partial}{\partial x_j}\left[\left(\mu+\frac{\mu_t}{\sigma_\varepsilon}\right)+\frac{\partial\varepsilon}{\partial x_j}\right]+C_{1\varepsilon}\frac{\varepsilon}{k}(G_k+C_{3\varepsilon}G_b)-C_{2\varepsilon}\rho\frac{\varepsilon^2}{k}+S_\varepsilon \tag{13}$$

where G_k is the generation of turbulence kinetic energy term caused by the gradient of the main velocity. G_b is the generation of the turbulence kinetic energy due to buoyancy. Y_M account for the addition of the fluctuation dilatation in turbulence to the overall dissipation rate. $C_{1\varepsilon}$, $C_{2\varepsilon}$ and $C_{3\varepsilon}$ represent the model constants. σ_ε is the Prandtl number associated with the kinetic energy and dissipation rate. S is a user-defined functions that can be used to modify both terms. The default values for the constants as well as the Prandtl number were used. No user-defined terms were included. The Standard $k-\varepsilon$ is mainly used for high Reynolds number applications.

3.3.2 RNG $k-\varepsilon$ model

An improved version of the Standard k-ε model is the statistically derived model using the Re-normalization group theory the RNG $k-\varepsilon$ model. This model includes several modifications on the standard model to improve it is accuracy in some flow cases. The RNG model contains an additional term to increase the accuracy of rapidly strained flows. It includes the effect of swirl on turbulence which significantly increases the accuracy of swirling flows. Unlike the standard model who uses a constant value for the Prandtl number, the RNG model calculate the Prandtl numbers based on analytical formula. Finally, RNG model provides an analytical formula for the effective viscosity which allows it to account for low Reynolds number effect upon the correct near-wall modelling. The RNG model has a similar transport Equation for k and ε but with few modifications as shown in Equations (14) and (15).

$$\frac{\partial}{\partial t}(\rho k)+\frac{\partial}{\partial x_i}(\rho k u_i)=\frac{\partial}{\partial x_j}\left(\alpha_k \mu_{eff}\frac{\partial k}{\partial x_j}\right)+G_k+G_b-\rho\varepsilon-Y_M+S_k \tag{14}$$

$$\frac{\partial}{\partial t}(\rho\varepsilon)+\frac{\partial}{\partial x_i}(\rho\varepsilon u_i) =\frac{\partial}{\partial x_j}\left(\alpha_\varepsilon \mu_{eff}\frac{\partial \varepsilon}{\partial x_j}\right)+C_{1\varepsilon}\frac{\varepsilon}{k}(G_k+C_{3\varepsilon}G_b)-C_{2\varepsilon}\rho\frac{\varepsilon^2}{k}-R_\varepsilon+S_\varepsilon \tag{15}$$

where α here represent the inverse effective Prandtl number that is derived analytically and R_ε here is the extra term used to account for the effect of rapidly strained flows.

3.3.3 Standard $k-\omega$ model

The standard $k-\omega$ model is based on the Wilcox model to account for low-Reynolds number, compressibility and shear flow. The two transport Equations are in terms of turbulence kinetic energy, k ,and specific dissipation rate, ω.

$$\frac{\partial}{\partial t}(\rho k)+\frac{\partial}{\partial x_i}(\rho k u_i)=\frac{\partial}{\partial x_j}\left(\Gamma_k \frac{\partial k}{\partial x_j}\right)+G_k-Y_k+S_k \tag{16}$$

$$\frac{\partial}{\partial t}(\rho \omega)+\frac{\partial}{\partial x_i}(\rho \omega u_i)=\frac{\partial}{\partial x_j}\left(\Gamma_\omega \frac{\partial \omega}{\partial x_j}\right)+G_\omega-Y_\omega+S_\omega \tag{17}$$

where Γ, represents the effective diffusivity. One of the main disadvantages in this model is it is strong sensitivity to freestream conditions. Therefore, it is used to model near-wall regions only where regions of interest are within the shear layer.

3.3.4 SST $k-\omega$ model

The shear-stress transport model offers many modifications on the standard $k-\omega$ model. It includes an additional term that is used as a damped cross-diffusion term. It also incorporates the $k-\varepsilon$ into the $k-\omega$ by using a blending function. This activate the $k-\varepsilon$ in the freestream region and the $k-\omega$ in the near wall region. The SST model also accounts for the transport of the turbulent shear stress and incorporates it in calculating the turbulent viscosity. The kinetic transport Equation is the same as Equation (17). However, the specific dissipation Equation is as follows:

$$\frac{\partial}{\partial t}(\rho \omega)+\frac{\partial}{\partial x_i}(\rho \omega u_i)=\frac{\partial}{\partial x_j}\left(\Gamma_\omega \frac{\partial \omega}{\partial x_j}\right)+G_\omega-Y_\omega+D_\omega+S_\omega \tag{18}$$

where D represents the cross-diffusion term.

3.3.5 Transition SST model

The transition SST model is based on the SST $k-\omega$ and two other transport Equations. The first one deals with the intermittency which is observed in turbulent or

near the transition to turbulence flows. The second one is in terms of momentum-thickness Reynolds number. More details about this model can be found in [48].

3.4. Mesh Generation, Independence Study and Validation

A non-uniform structured mesh is generated using the commercial software POINTWISE. The near wall region was modelled carefully to assure that the film layer is modelled correctly. Near wall modelling is required when using $k-\varepsilon$ models with Enhanced Wall Function (EWF). However, for the k-ω related turbulence models no wall model is required as wall modelling is already included in its formulation. To properly resolve the shear stress and heat transfer near the wall, it is required for all turbulence models to have a y^+ value of unity near the wall. The y^+ represents a non-dimensional distance of first node near the wall which depends on the friction velocity. The y^+ is related to the first element height (y) with velocity friction (u_τ) and kinematic viscosity (ν) as follows: $y^+ = yu_\tau/\nu$. Meanwhile, the velocity friction is calculated as $u_\tau = \sqrt{\tau_w/\rho}$. The height of the first cell closest to the wall has been calculated to be at least $0.000170D$ to achieve the y^+ constraint. Figure 3 shows the generated mesh. The maximum skewness for the generated mesh shown in Figure 3 is found around the value of 0.6 for a jet angle of 30°. As the jet angle decreases, the skewness decreases which reduce numerical error.

Three meshes have been generated and tested. The first tested mesh is a coarse mesh with 145,000 elements, the second mesh is with moderate mesh with 280,000 elements and the last mesh is a fine mesh with 500,000 elements. The RNG $k-\varepsilon$ with EWF turbulence model was selected for the grid independence study. Other turbulence models are assumed to give grid independent solution. The mesh independent study can be seen in Figure 4. As mentioned, the three different mesh sizes were tested. The result shows that there is no significant difference between the results for the fine and moderate mesh size. Both have a relative error in the value of the numerical results of Bayraktar and Yilmaz [25] of 1.7%. The coarse mesh had a relative error of about 4.5%. The moderate size mesh with the size of 280k elements were selected in this study.

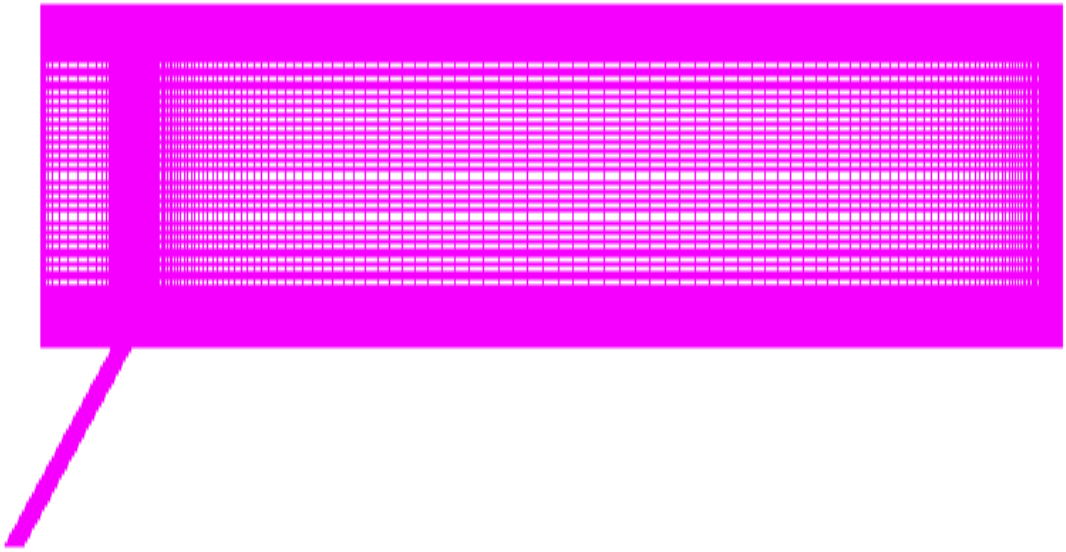

Figure 3: Grid used for the analysis

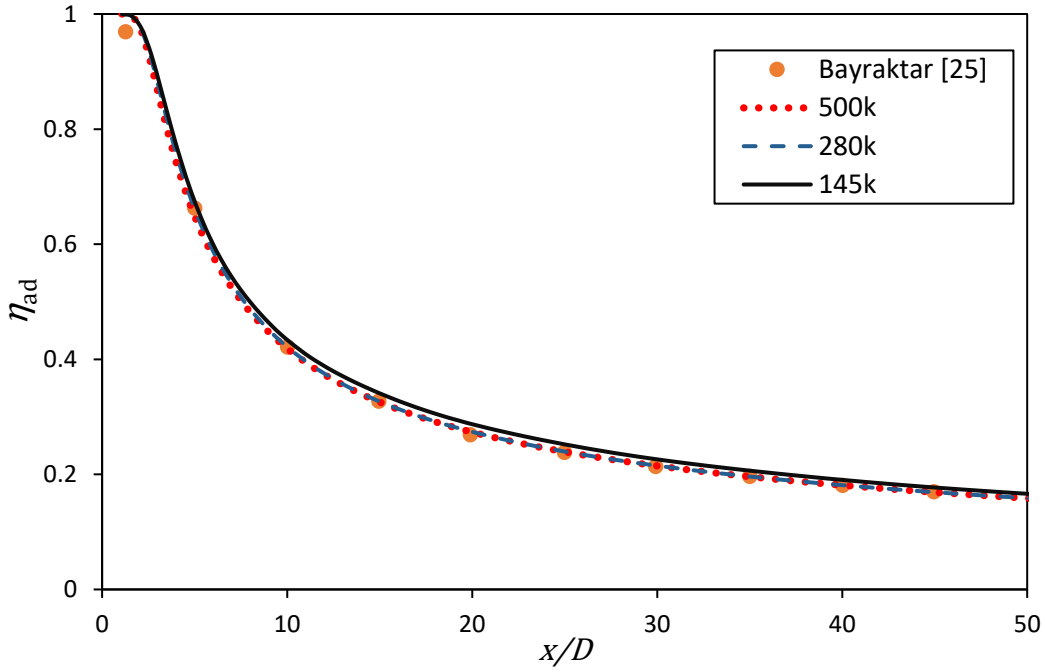

Figure 4: Mesh independence of the numerical model

In validation, the finer mesh was used. This work was validated using the numerical work of Bayraktar and Yilmaz [25] and the experimental work of O'Malley [27]. The same flow parameters were used as mentioned in Table 1.

Table 1: Flow parameters used in this study.

Run	V_c	V_h	M	$T_c\ (K)$	$T_h\ (K)$
Validation	2.3	23	0.13	300	373
1	2.5	30	0.1	300	360
2	7.5	30	0.3	300	360
3	12.5	30	0.5	300	360
4	20	30	0.8	300	360
5	25	30	1	300	360
6	50	30	2	300	360

The numerical validation against the numerical analysis in ref [25] using the flow parameters in Table 1 is shown in Figure 5. The results from the numerical model are in an agreement with the published work as the model is sufficiently predicting the behavior for the entire downs-stream length. Figure 6 shows the experimental validation of the current model against the experimental work of O'Malley [27] and the numerical work of Bayraktar and Yilmaz [25]. The model was able to predict the velocity profile at two different downstream distances, 1.3 and 3 *D* from the slot. The slope of the first two points in Figure 5 shows the gradient of the velocity in the first cell. This gradient matched the values in the experimental work of O'Malley [27]. These two results show that the model has have shown an excellent agreement in capturing fluid and heat transfer related parameters.

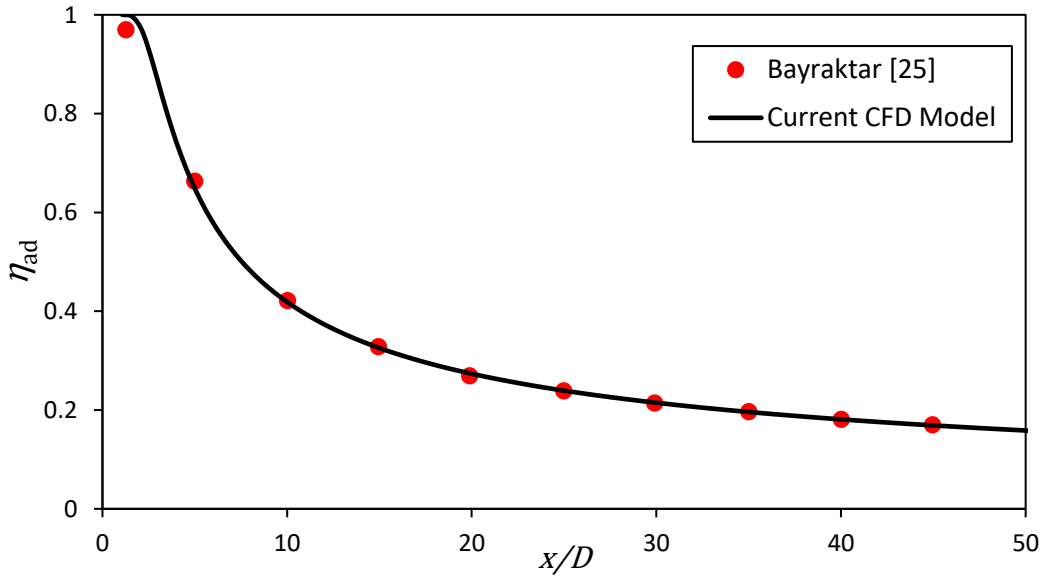

Figure 5: Numerical model results against the numerical study of Bayraktar and Yilmaz [25]

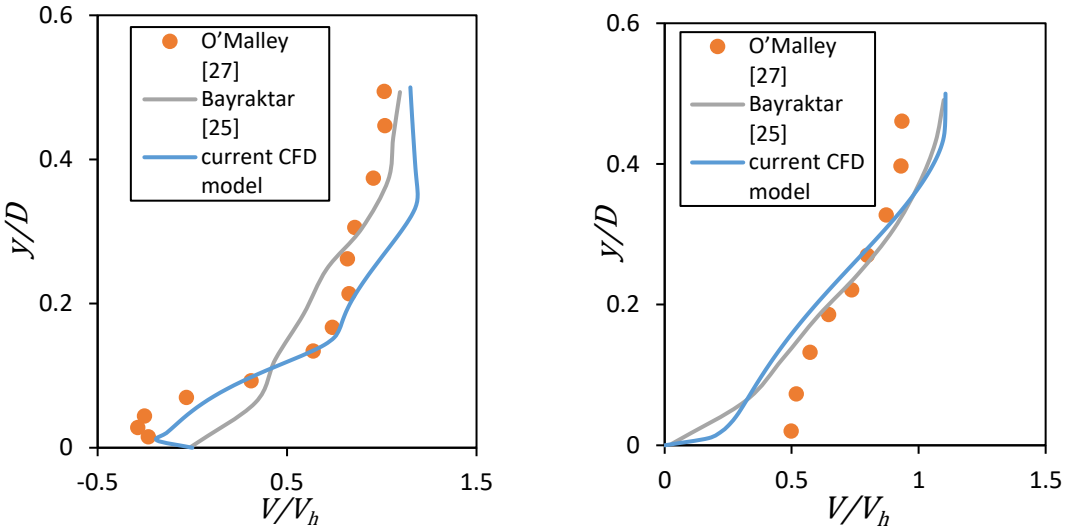

$x/D = 1.3$ $x/D = 3.0$

Figure 6: Experimental validation against O'Malley [27] experimental results

Chapter 4. Results and Analysis

In this chapter, the results of this study are presented, starting with turbulence model selection. Then, a parametric study is performed to evaluate the effect of flow blowing ratio, film injection angle and fluid density ratio on the AFCE and the effect of interrelation between these parameters are explored using response surface methodology (RSM). The study at the end discussed the impact of centrifugal force and wall thermal conductivity on the AFCE. The impact of film hole diameter, centrifugal force and wall thermal conductivity are not explored with other parameters since they have minimal intercorrelation with other parameters. The wall thermal conductivity is explored using conjugate heat transfer for different wall thermal conductivity values, which represent different blade material.

4.1. Turbulence Model Selection

A comparative analysis of turbulence models in Section 3.3 is carried out here to select an optimum option that predicts the AFCE that match published results. The selected model is later used in the rest of the thesis work. In this regard, various turbulence models are compared in Figure 7. As illustrated in the figure, all the models show the same trend in the AFCE curves. However, $k-\varepsilon$ models show the best accuracy in the reported AFCE.

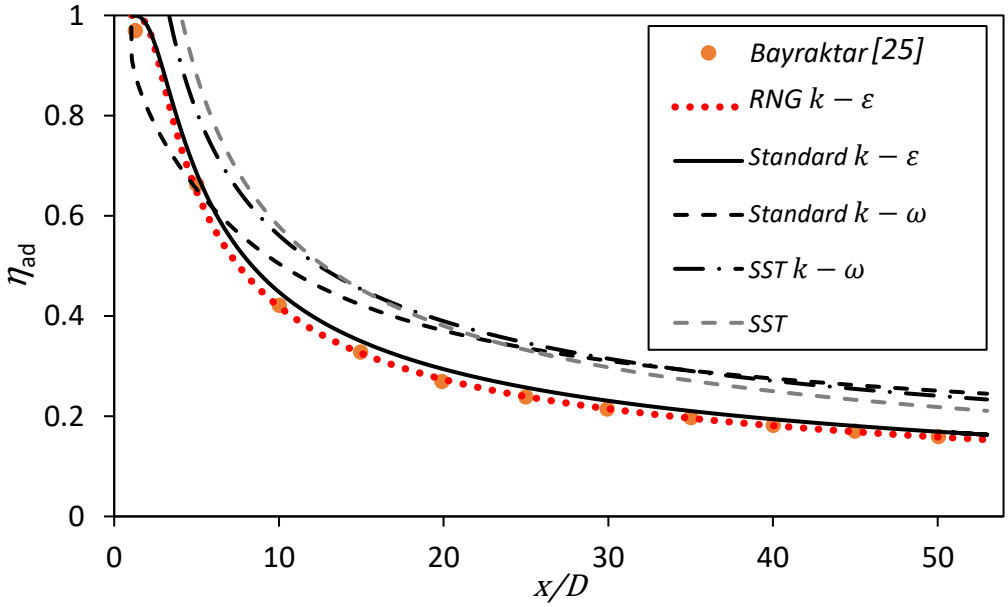

Figure 7: Turbulence model selection based on the validation case in Table 1.

The RNG $k-\varepsilon$ model shows the best accuracy with an overall deviation of 1.7% from the numerical results reported by Bayraktar and Yilmaz [25]. This is followed by the standard $k-\varepsilon$ model with a deviation of 6.21%. The other turbulence models show relatively higher deviation from the $k-\varepsilon$ models. The standard $k-\omega$ results in a 26.4% deviation, while the SST $k-\omega$ shows 26.84% deviation. Finally, the SST model yeilds 27.6% deviation. Since the reported AFCE depends only on the wall temperature as evident in Equation (2), the accuracy of the turbulence model depends on how the boundary layer of film cooling is modelled. The RNG $k-\varepsilon$ model with EWF reports the best accuracy, since the effective turbulence viscosity is considering the low-Reynolds number effects close to the wall. Therefore, the RNG $k-\varepsilon$ model is adopted as the turbulence model to simulate the current problem and to understand the intercorrelation between different parameters.

4.2. Parametric Study

Three main intercorrelated parameters affecting the AFCE are closely examined in this section, which are flow blowing ratio (M), film injection angle (α) and fluid density ratio (DR). Different combination of these intercorrelated parameters have been formed as listed in Table 2. The effect of blowing ratio has been explored under wide range of values from 0.1 to 0.2. All the sets in Table 2 have been tested for three film injection angles of 30°, 60° and 90°. This has been also tested against three different fluid density ratios of $DR = 1.2$, 2.0 and 3.0. The variation of DR values has been modeled using three different mainstream air temperatures as shown in Table 3.

Table 2: Analysis set with different selected parameters.

Sets No.	$\boldsymbol{V_c}$ $[m/s]$	$\boldsymbol{V_h}$ $[m/s]$	$\boldsymbol{M}$
1	2.5	30	0.1
2	7.5	30	0.3
3	12.5	30	0.5
4	20	30	0.8
5	25	30	1
6	50	30	2

Table 3: Density ratios of coolant to mainstream gas as function of temperature.

DR	T_h $[K]$	T_c $[K]$
1.2	360	300
2.0	600	300
3.0	900	300

4.2.1 Film cooling performance curves

It is expected that as the mainstream hot fluid flows in the x-direction, more heat will be transferred to the wall due to enhanced flow mixing between the hot fluid in mainstream and the relatively cold fluid injected by film hole. Hence it is expected that the wall temperature will converge to the hot mainstream temperature. As the wall temperature approaches the mainstream temperature, the adiabatic film cooling effectiveness decreases as shown in Figures 8 to 10. The temperature of the film formed by the discharged cold flow increases due to the heat transfer that occurs between the hot mainstream flow and the surface. Hence, film cooling effectiveness in shielding the wall decays along the x-direction. For film cooling injection angle of 30°, Figure 8 shows that the adiabatic film cooling effectiveness has non-monotonic relation with blowing ratio (M), while a monotonic relation is found for 60° and 90° (as shown in Figures 9 and 10, respectively). An increase in AFCE with blowing ratio is expected since more fluid discharges from the film hole and bigger blanket of cool air is formed between the hot mainstream flow and the surface causing better surface shielding. However, this trend is not indefinite since as film discharge increases beyond $M = 0.8$ (for blowing angle of 30°), the chance of film detachment from the surfaces increases causing improper protection and less effectiveness in forming a cool film that shields the surface from the hot mainstream. The blowing ratio at which the AFCE starts to fall afterwards is identified in this study as the critical blowing ratio. In the first case of variable injection angles and $DR = 1.2$ shown on Figures 8 to 10 the critical blowing ratio is $M = 0.8$. As the blowing ratio approaches to the critical blowing ratio, the overall raise in AFCE decreases. Similarly, as the blowing ratio increases beyond the critical blowing ratio; the overall decrease in the AFCE curve increases. These trends can be seen clearly in Figure 8. Hence maximum AFCE for $DR = 1.2$ and $\alpha = 30°$ is achieved at $M = 0.8$.

The rate of deterioration in AFCE with x-direction is high at the beginning and then this rate starts to decrease. The main reason for such high rate of deterioration in AFCE near the film hole is the thin boundary layer formed by the cool film, which starts to grow as flow moves in x-direction. Still the AFCE keeps dropping since heat transfer between the mainstream and surface is more pronounced compared to the boundary layer shielding effect.

The effect of film cooling detachment is clearly seen in Figure 10 (with film injection angle of 90°). As shown in Figure 10, the local AFCE directly after the hole is lower in for the 90° case compared to the 30°case. More details regarding injection angle effect is discussed in Figure 11.

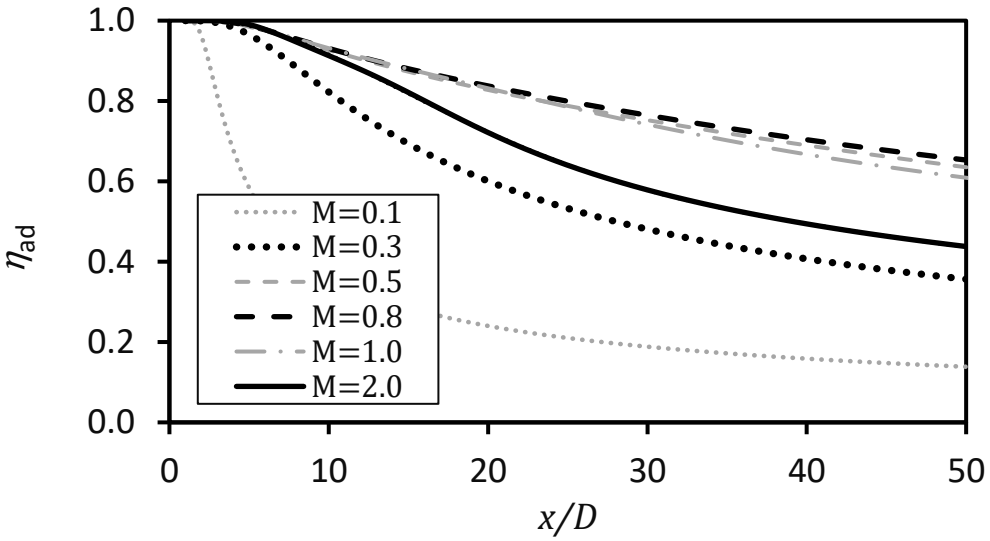

Figure 8: AFCE for DR=1.2 and α=30

Figure 11 shows that the effect of the injection angle is negligible at a low blowing ratio of $M = 0.1$. The overall AFCE is also relatively lower at low blowing ratios, which can be seen in Figure 11 (a to d). A low blowing ratio means less film cooling fluid is being injected to the main stream, which explains the lower the surface protection and hence the lower the AFCE of the surface. At low blowing ratios, the injection angle has low to no-effect on forming the film blanket which will mainly be dominated by the mainstream flow boundary layer. A comprehensive view shows that a low blowing ratio means the flow has low momentum and energy to affect the mainstream flow field, which reduces the effect of the injection angle. However once blowing ratio increases beyond $M = 0.1$, the injection angle becomes an important

factor that can alter the flow field. The effect of blowing ratio is complex since it relates quantitatively the effect of flow linear momentum of two streams without counting the effect of direction of these quantities. Linear momentum is a vector parameter and its impact on the flow field is determined by the quantitative value and the flow vector direction. For blowing ratio equal to 1 or less, as shown in Figure 11 (a to c), the AFCE increases as the blowing angle decreases. Smaller angles indicate a higher chance that the flow remains in contact with the surface forming a cool blanket and it properly shields the surface from the hot mainstream. However, once a high blowing ratio of $M = 2.0$ is used, as shown in Figure 11d, the angle effect becomes less important and the previous relation fails. Figure 11d shows that the AFCE is the highest for a blowing angel of $60°$, which assures the presence of maximum AFCE between $30°$ and $90°$ in the downstream region. This behavior indicates that as blowing ratio increases, more mass of cool fluid becomes available to shield the surface from the hot mainstream. At high injection angle of $90°$ the chance of detachment is high and at low angle of $30°$ the thickness of cool air blanket is small. In contrast, at angle of $60°$, the flow is attached to the wall, forming a thick blanket, and is more sustained. In general, for a wide blowing ratio range of $M = 0.1 - 1.0$, decreasing injection angle causes an increase in AFCE that means film attachment is dominating the wall shielding. On the other hand, at high blowing ratio of $M = 2.0$, higher angles form a thicker cooling film that dominates the heat transfer. However, increasing injection angle to obtain a thicker film eventually causes detachment of cooling film and deterioration of the AFCE. In conclusion, the injection angle has two conflicting effects on AFCE. A small injection angle provides a low chance of fluid detachment but a thin blanket of cool fluid. Also, a high blowing angle results in a high chance of detachment but offers a thicker blanket of cool fluid. Note that, these contradicting effects depend on the blowing ratio as well. Finally, by using Equation (3b), one can study the effect of changing the density ratio at a constant blowing ratio by changing the velocity ratio. Using Equation (3b), the effect of density ratio is studied while keeping the injection angle at a constant value of $30°$. Figure 12 shows the effect of density ratio (DR) at different blowing ratios. At low blowing ratios, Figure 12 (a and b), increasing the DR reduces the overall AFCE. The density ratio (DR) represents the density ratio between the relatively cool fluid and the mainstream hot fluid.

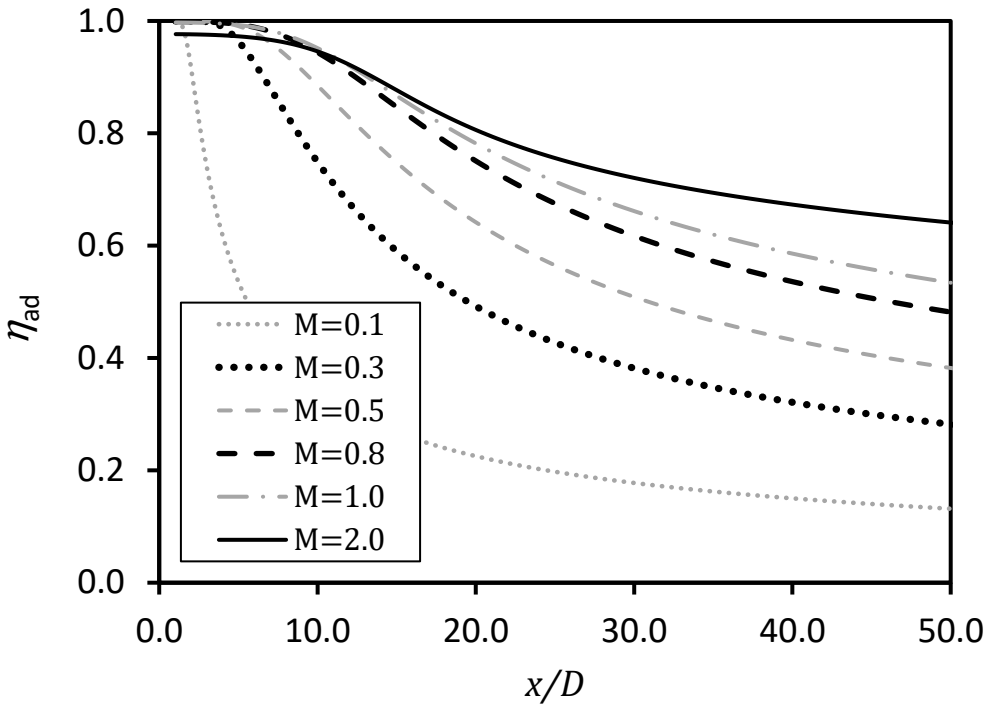

Figure 9: AFCE for DR=1.2 and α=60

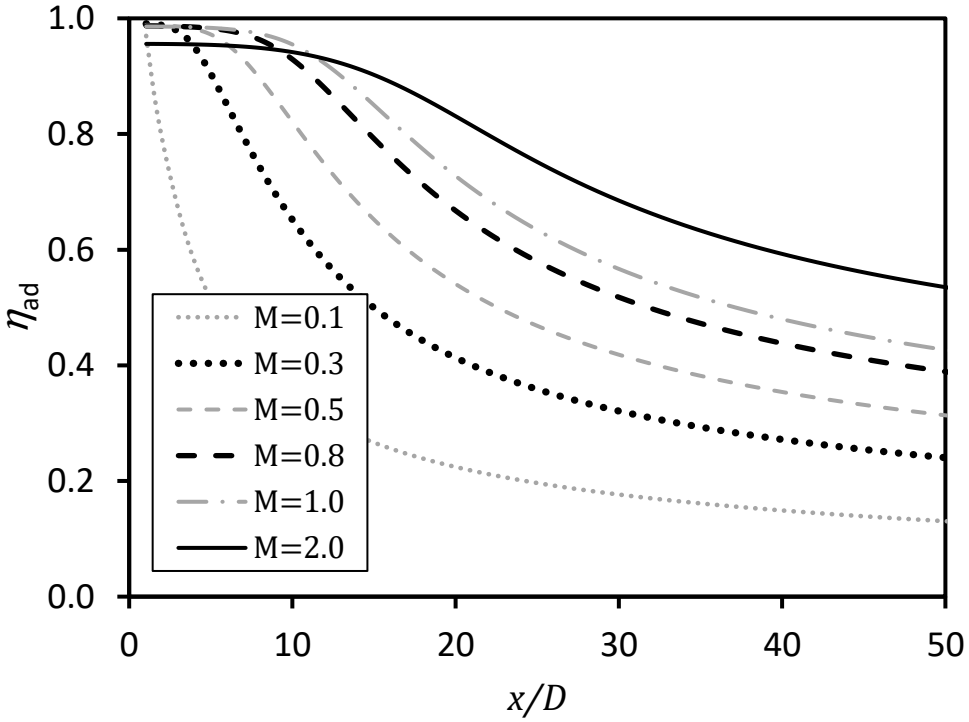

Figure 10: AFCE for DR=1.2 and α=90

The DR has two conflicting effects on heat transfer between mainstream hot fluid and the blade surface. As density ratio increases the velocity ratio (VR) decreases causing a lower linear momentum of injected cooling fluid, which decreases the size of

the film cooling blanket covering the blade surface. So, increasing density ratio means a lower protection for the blade surface.

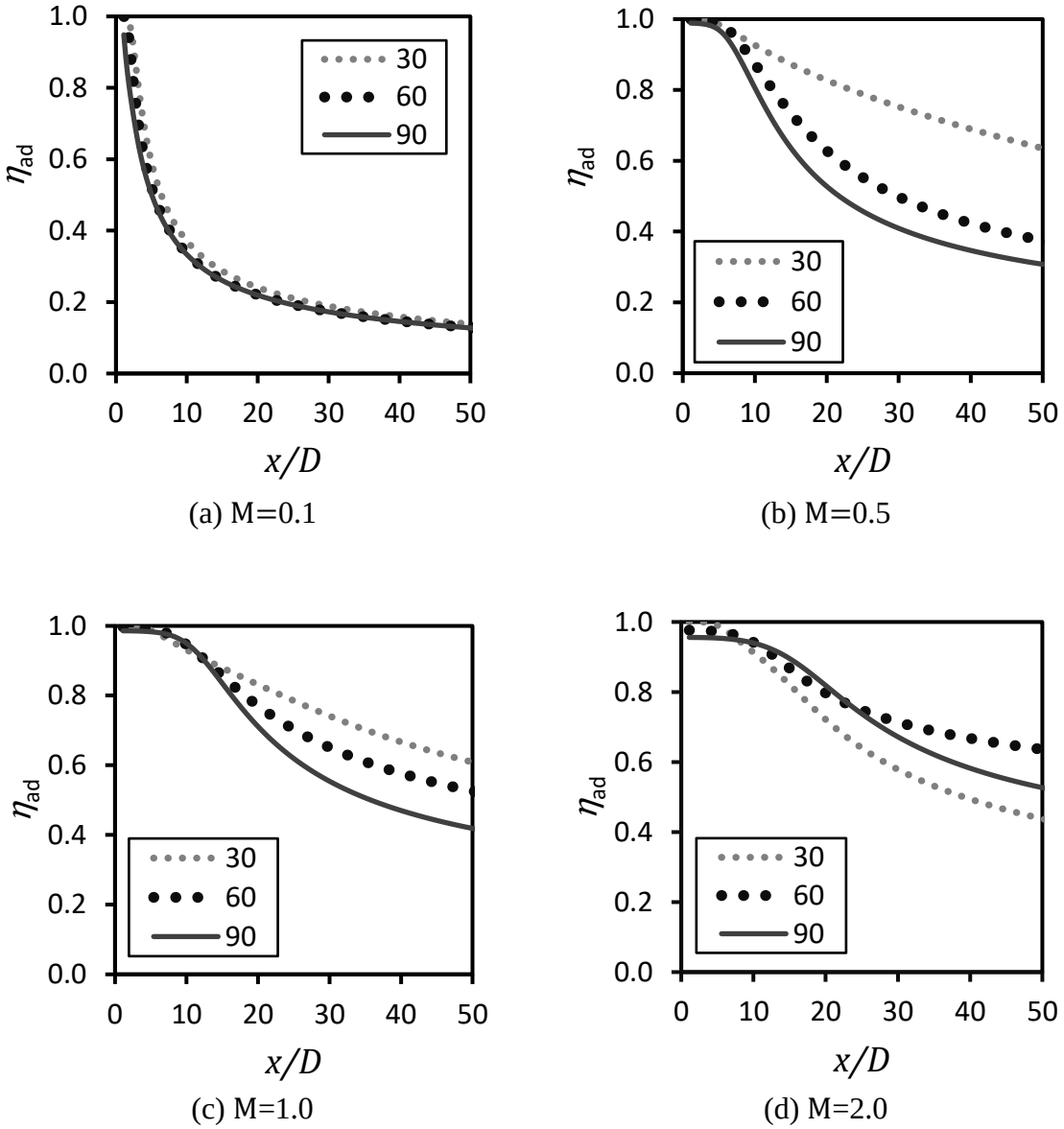

(a) M=0.1 (b) M=0.5

(c) M=1.0 (d) M=2.0

Figure 11: AFCE for DR=1.2 at various angles and blowing ratios

The second effect is that as density ratio increases the thermal capacity of the cooling flow increases, which allow it to carry more thermal energy and prevents such energy from reaching the surface. The increase in thermal capacity of the cooling fluid shields the surface from additional heat transfer and hence boosts AFCE. Figure 13 shows that as DR increases the AFCE decreases for low M values due to the very low thickness of film cooling blanket. However, for high M values, as DR keeps increasing, the effect of thermal capacity of cooling fluid increases which causes a better shielding

against heat transfer from mainstream hot fluid which yields better AFCE. At blowing ratio of $M = 1.0$, see Figure 12c, the enhancement in AFCE due to the increase of DR starts to appear and become obvious at a higher blowing ratio of $M = 2.0$ in Figure 12d. The highest DR shows the highest performance as seen in Figure 12d, in which the DR is increased by a factor of 3 and the VR is reduced by the same factor to keep the blowing ratio constant. For injection angle of 30°and DR=1.2 the critical blowing ratio was reported as $M = 0.8$ in Figure 8. However, the increase in the DR increases the critical blowing ratio as can be seen in Figure 12d and 13. The critical blowing ratios are $M = 0.8$, $M = 1.0$ and $M > 2.0$ for $DR = 1.2$, $DR = 2.0$ and $DR = 3.0$, respectively. The coolant jet velocity streamlines at various film cooling configurations are shown in Figure 14. The coolant jet streamlines starting from jet entrance are used to describe the effect of the interrelated parameters on AFCE. Figure 14 (a to d) shows the effect of coolant injection angle and blowing ratio on the coolant jet velocity streamlines. Blowing ratio effect on the film cooling blanket are shown in Figure 14 (a and c). Higher blowing ratio often results in a higher thickness of the film cooling blanket which can affect the AFCE positively or negatively as discussed earlier. The effect of coolant injection angle on the film cooling thickness is shown in Figure 14 (b and d). Higher coolant injection angles show a higher thickness of the film cooling blanket. However, higher coolant injecton angles inject the coolant away from the turbine's blade which result in a higher heat transfer between the mainstream gas and the film coolant blanket due to higher blockage of the mainstream gas flow which reduces the overall AFCE. Lower local AFCE are also presented in the case of high angles, which increase the chances of turbine blade failure due to thermal stresses around the film cooling slot.

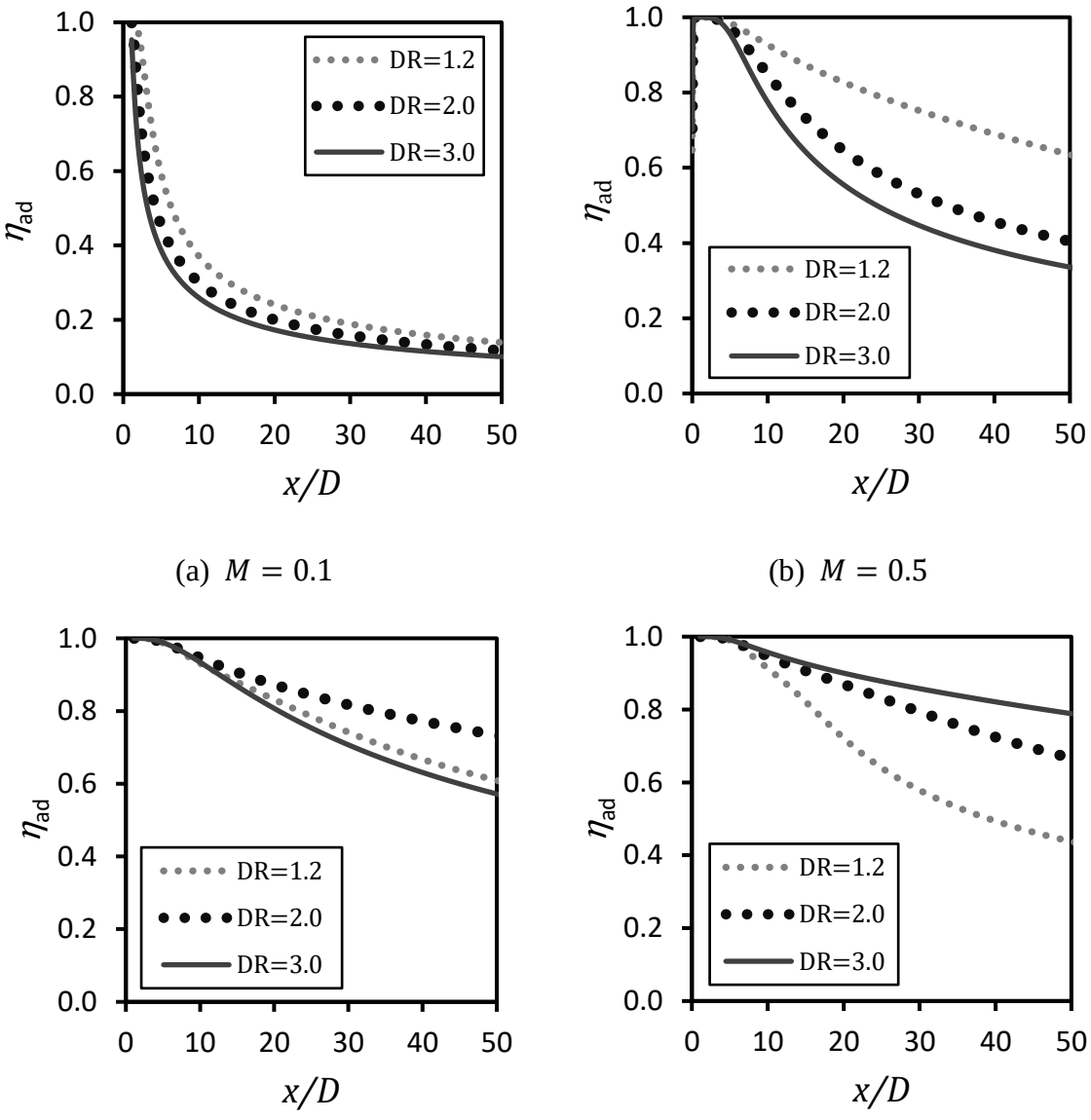

(a) $M = 0.1$ (b) $M = 0.5$

(c) $M = 1.0$ (d) $M = 2.0$

Figure 12: AFCE at different blowing ratios and an injection angle of 30°

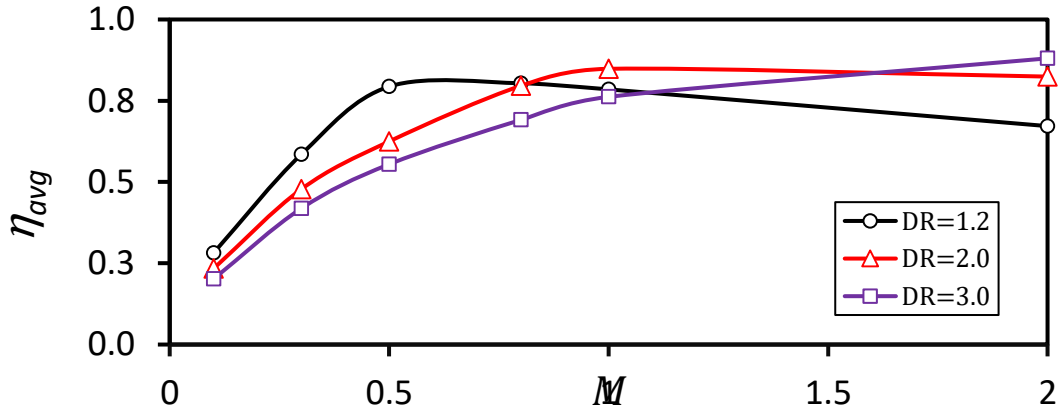

Figure 13: Variation of average AFCE with blowing ratio at three different DR values

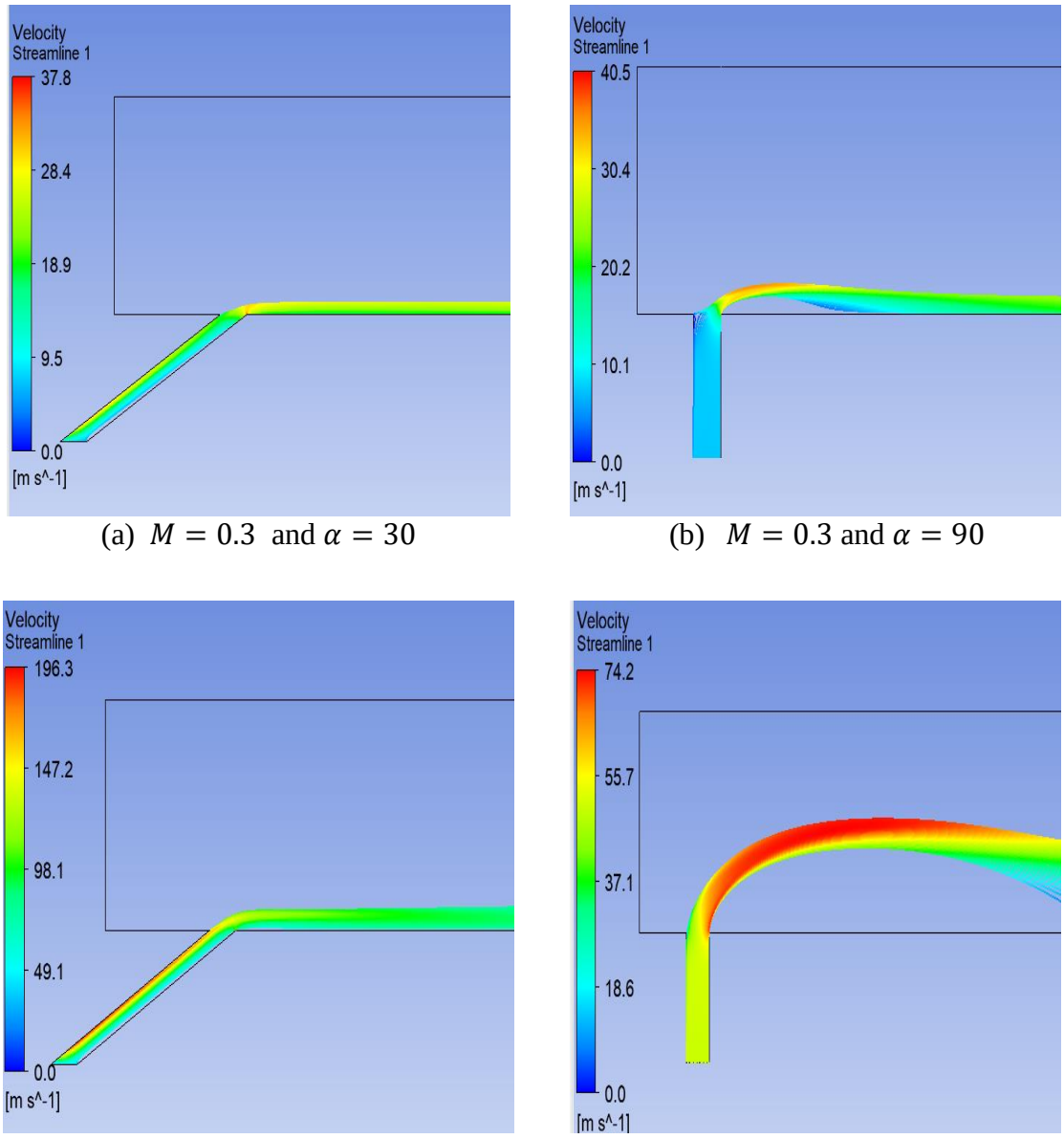

(a) $M = 0.3$ and $\alpha = 30$ (b) $M = 0.3$ and $\alpha = 90$

(c) $M = 2.0$ and $\alpha = 30$ (d) $M = 2.0$ and $\alpha = 90$

Figure 14: Velocity streamlines from the coolant jet

4.2.2 Surface response

To explore a relationship between several interrelated parameters affecting the AFCE, response surface methodology (RSM) is used. RSM is a group of statistical and mathematical models that are used in analyzing a model where a response of interest is affected by several interrelated parameters [49]. In this work, the averaged AFCE is the response of interest and the independent variables are blowing ratio, injection angle and density ratio. The averaged AFCE is defined as shown in Equation (2b) which represents the area weighted average of AFCE. In RSM analysis, all factors must be

reported for at least three different levels. In this work, four levels of the blowing ratio, three levels of injection angles and three levels of density ratio are considered in the RSM analysis. Table 4 shows the different levels of the independent variables.

Table 4: Levels of the independent variables used in the RSM.

Levels / ***Variables***	*Low*	*Medium*	*High*
M	0.1	0.5, 1.0	2.0
α	30	60	90
DR	1.2	2.0	3.0

This combination of parameters results in 36 reported averaged AFCE values. More levels are taken for the blowing ratio to increase the resolution of the RSM model in capturing the blowing ratio effect. RSM statistically measures the contribution of all the variables on the area weighted average AFCE. It reports the solely effect of a parameter, known as the main parameter effect and how the different parameters are interacting with each other. These models are generally performed using a statistical software. In this study, a commercial software named MINITAB is used to develop the RSM model and to determine the effect of the variables in Table 4 on the averaged AFCE. The significance of a term is identified by its corresponding *P-value.* Lower *P-value* is a characteristic of a significant term that has a big influence on the reported response value. In this model, the significance of blowing ratio, injection angle and the density ratio on the averaged AFCE is investigated. In practice, any variable that has a *P-value* less than 0.1 is considered significant. Table 5 shows the summary of the RSM model generated by MINITAB. The table shows that the terms M, M^2, α and $M * DR$ have the highest effect on the averaged AFCE.

The RSM generated regression model used to describe the averaged AFCE is shown in Equations (22) and (23). Equation (22) correlates the effect of all the terms on the averaged AFCE. While, Equation (23) is generated using the terms in Table 5 that have a *P-value* of 0.10 and below. The relative error in estimating the AFCE is 7.90% and 7.97% for Equations. (22) and (23), respectively. Therefore, Equation (23) can be used to accurately estimate the average AFCE within the minimum and maximum levels of the three different parameters in Table 4.

Table 5: RSM model summary.

Term	**Effect**	**Coef**	***SE Coef***	***T-Value***	**P-Value**
M	0.532	0.266	0.013	20.400	0.000
α	-0.101	-0.050	0.012	-4.170	0.000
DR	-0.039	-0.019	0.012	-1.590	0.123
M^2	-0.508	-0.254	0.023	-11.260	0.000
α^2	0.026	0.013	0.021	0.630	0.534
DR^2	0.006	0.003	0.021	0.140	0.890
$M * \alpha$	-0.006	-0.003	0.016	-0.180	0.862
$M * DR$	0.079	0.039	0.016	2.500	0.019
$\alpha * DR$	0.008	0.004	0.014	0.280	0.784

$$\eta_{avg} = 0.471 + 0.7800\,(M) - 0.00361\,(\alpha) - 0.094\,(DR) - 0.2815\,(M^2) + 0.000014\,(\alpha^2) + 0.0036\,(DR^2) - 0.000097\,(M) * (\alpha) + 0.0461\,(M) * (DR) + 0.000148\,(\alpha) * (DR) \quad (22)$$

$$\eta_{avg} = 0.4012 + 0.7742(M) - 0.001671\,(\alpha) - 0.0697\,(DR) - 0.2815\,(M^2) + 0.0461\,(M * DR) \quad (23)$$

The blowing ratio has two terms (M, M^2) in the generated regression model, which have opposing effect on the overall averaged AFCE. Increasing the blowing ratio (M) increases the AFCE until the squared term (M^2) starts to affect the AFCE negatively. The model also shows that increasing the injection angle will decrease the AFCE. The density ratio can contribute positively to the AFCE at higher values of the blowing ratio. These results are in agreement with the results discussed in section 4.2.1.

Figure 14 shows the interaction of three different variables. Figure 14 (a and b) suggest that the highest value of AFCE is achievable by working at lower values of injection angles and density ratios. Figure 14c shows that working at high values of blowing ratio achieve high AFCE regardless of the DR value. The quadratic effect of the blowing ratio given by Equation (23) can be seen in Figure 14a, where a negative effect on the AFCE is introduced.

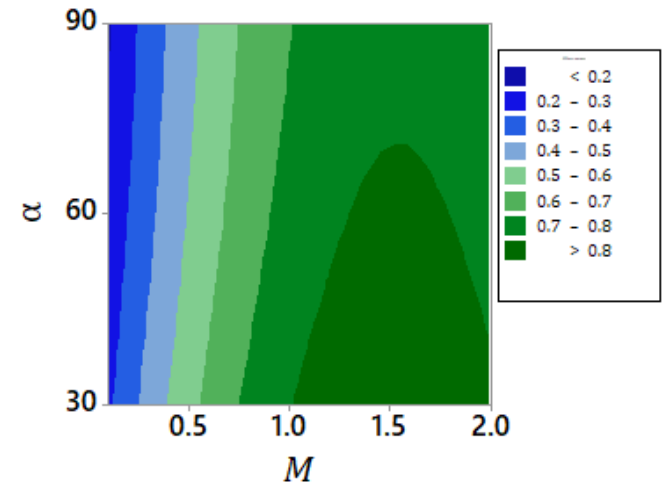

(a)

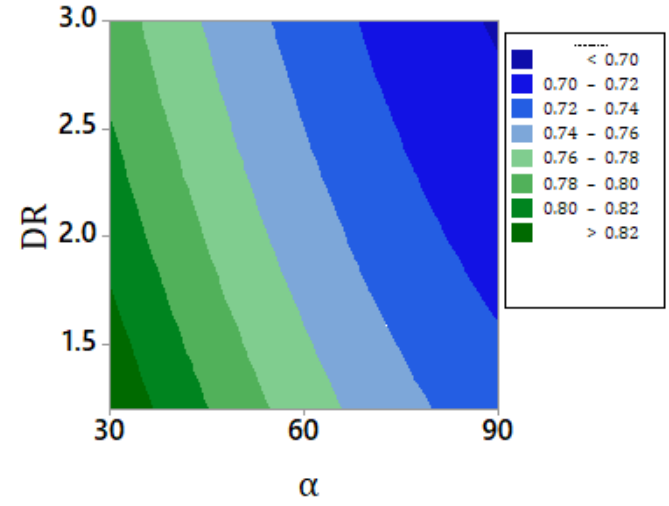

(b)

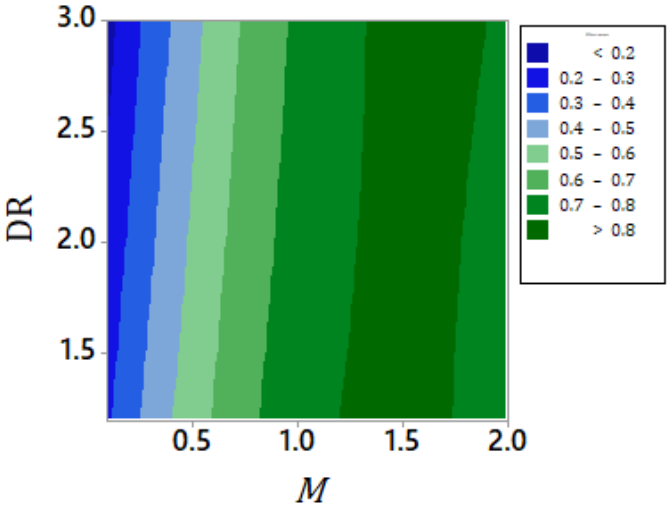

(c)

Figure 15: Contour plots of the averaged AFCE for all the parameters. (a) Blowing ratio for different injection angles at $DR = 1.2$, (b) Injection angle for different density ratios at $M = 1.0$ and (c) Blowing ratio for different density ratios at $\alpha = 30$

4.3 Jet Reynolds Number Effect on AFCE

The effect of jet Reynolds number on AFCE is investigated in this work by changing the jet diameter. Reynolds number is calculated using Equation (24):

$$Re = \rho VD/\mu \tag{24}$$

To eliminate the effect of the different affecting parameters, the numerical domain is kept constant, $L = 240$ mm, and the following film cooling configuration are selected: $M = 0.8$, $DR = 1.2$ and $\alpha = 30^o$. The mainstream Reynolds number is 6.7×10^5 and the jet diameters are 20 mm and 4 mm. The jet Reynolds number are 5.1×10^4 and 1.09×10^4, respectively. Figure 16 shows that as the jet diameter decreases, Reynolds number decreases, the AFCE decreases. The larger the film holes mean more mass is allowed to contribute to the film cooling resulting in a thicker film cooling blanket. Thicker film cooling provides better shielding compared to thin blanket even at the same jet Reynolds number since thicker film provides better heat removal from the mainstream. The film effectiveness in cooling the surface is boosted by the ability of the film in shielding the surface and carrying the heat from the hot mainstream and away from the surface.

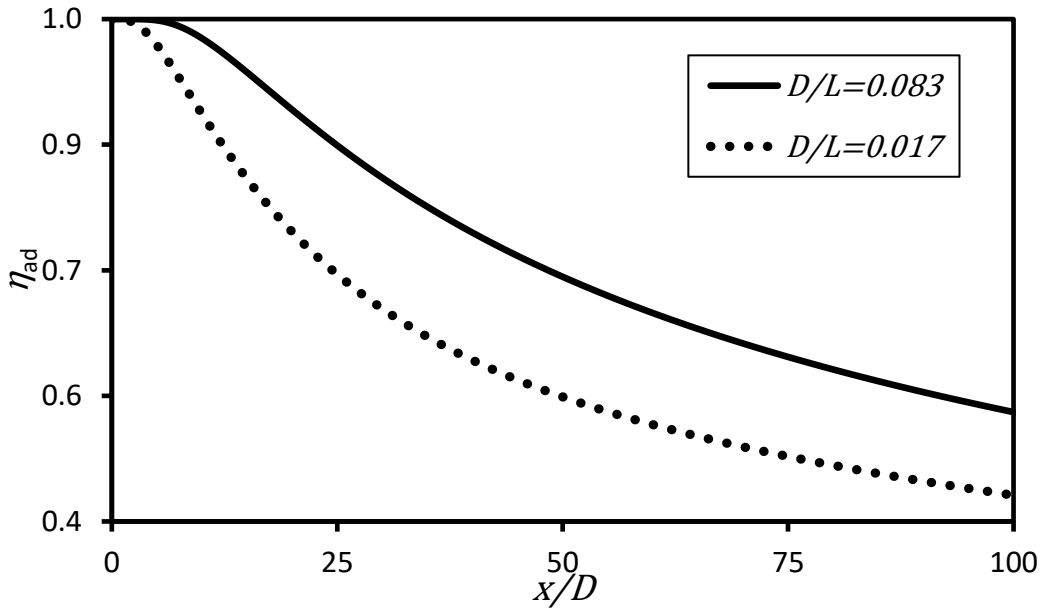

Figure 16: Jet diameter effects on the AFCE

4.4. Centrifugal Force Analysis

Centrifugal force is a body force that alters the flow field and affects the film cooling blanket attachment to the turbine's blade surface. The centrifugal force is related to the centripetal acceleration at the hole specific location and turbine rotational speed. The centripetal acceleration and force at a specific hole location are defined by Equations (25) and (26), respectively, as;

$$a_c = \omega_t^2 * r \tag{25}$$

$$F = ma_c \tag{26}$$

where, a_c is the centripetal acceleration, ω_t is the turbine angular acceleration, *r* is the location of the hole from the turbine's center and *m* is the turbine mass. As shown in Equation (25) the centrifugal force increases with the increase of the turbine angular velocity. In this study, the tip hole used to cool the tip of the blade is analyzed at different turbines rotational speeds. The direction of acceleration is pointing toward positive y-axis as shown in Figure 2 zone 3. Modern macro-gas turbine engines can operate at rotational speeds of about 15,000 RPM [50]. This high value produces a high centripetal acceleration at the tip that can reach up to $2.7 \times 10^6\ m/s^2$ on a two meters diameter turbine. In this work, the effect of centripetal acceleration on the AFCE is investigated. In ANSYS FLUENT the gravity module has been used to add the centripetal acceleration value in the y-direction.

Figure 17 shows the AFCE curves at different centripetal accelerations in m/s^2. The 0 m/s^2 results correspond to the case of AFCE at the following configuration, $M = 0.1$, $\alpha = 30°$ and $DR = 2.0$. As shown in Figure 16, as the centripetal acceleration increases the overall AFCE drops. At lower centripetal accelerations, the drop in the AFCE around the hole (lower than 5Ds) is considerably lower than that of downstream. However, at higher centripetal accelerations the opposite behavior is observed. In general, centrifugal forces lift the film cooling layer away from the wall and causes the AFCE to drop significantly. This is one of the main reasons for turbine blades fail due to overheating at the blade tip [51]. To prevent this thermal stress failure at the turbine blade tip, a non-uniform distribution, more biased toward the tip, of the film cooling holes must be used [51].

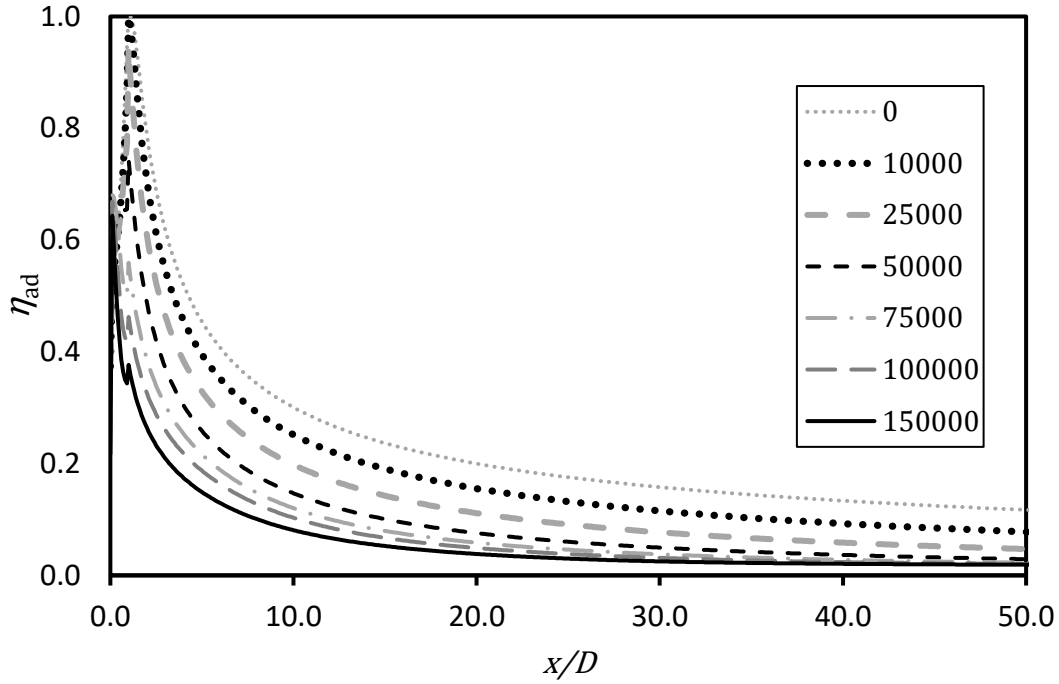

Figure 17: AFCE curves for different centripetal accelerations

4.5. Conjugate Heat Transfer Analysis

The AFCE is used to report the performance of film cooling parameters by assuming adiabatic walls. To study the effect of turbine blade material, conjugate heat transfer analysis is used and FCE is reported. Fist, the turbine blade walls and the coolant plenum are modeled. Then, fluid-solid and solid-fluid interfaces between the mainstream gas, the turbine blade and the coolant plenum are modelled using ANSYS FLUENT. Figure 18 shows a schematic of the formulated problem where the coolant enters the mainstream through the slot from the modeled plenum. Note that the rest of domain dimensions in the schematic are the same as in Figure 2. The wall thermal conductivity is investigated by using K_R value, the ratio of thermal conductivities of wall material and air at 360°C, as shown in Equation (27).

$$K_R = \frac{k_w}{k_{c@360C}} = k_w/0.03 \tag{27}$$

The different values of the tested wall thermal conductive are shown in Table 6. The results of the FCE using conjugate heat transfer analysis are compared to the AFCE (with $M = 0.1$, $\alpha = 90°$ and $DR = 1.2$) reported in [25] and [27]. The validation of the conjugate heat transfer analysis is considered when the reported FCE agrees with AFCE for the smallest ratio of $K_R = 1.0$.

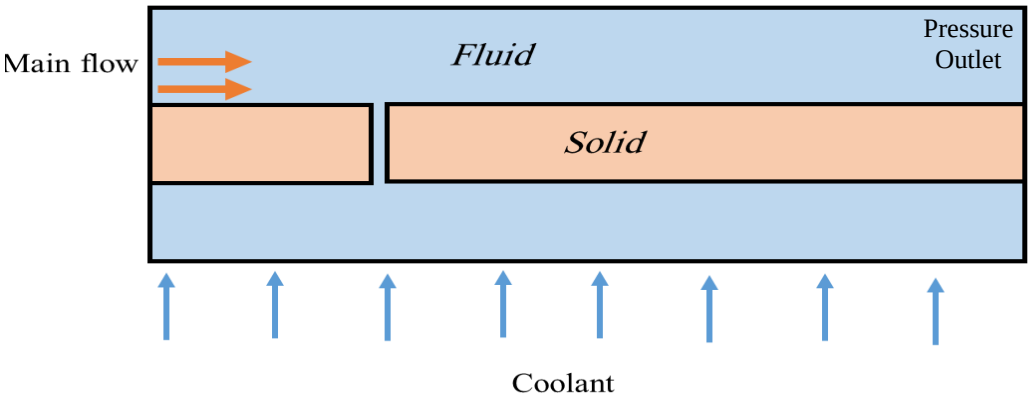

Figure 18: Schematic of the conjugate heat transfer analysis

Table 6: Thermal conductivity values of the blade wall.

K_R	$k_w\ (W/m.K)$
1	0.03
100	3
1000	30
10000	300

Various thermal conductivity values of the tested wall are shown in Table 6. The results of the FCE using conjugate heat transfer analysis are compared to the AFCE of $M = 0.1$, $\alpha = 90°$ and $DR = 1.2$. The wall thickness is 3.5D as shown in Figure 2. shows the results of the conjugate heat transfer analysis. These results for FCE for low thermal conductivity ratio ($K_R = 1$) are in agreement with the AFCE values in Section 4.2.1 of this study, and also validated with [25] and [27]. As evident from the figure, increasing the thermal conductivity ratio (K_R) leads to a decrease of the FCE in all regions for all cases. More heat is transferred between the mainstream gas and the coolant chamber by a higher thermal conductivity of the blade, which reduces the effective coolant temperature at the slot entrance. The coolant is then injected at a lower temperature and reduces the performance of film cooling significantly.

Multiple holes are used to improve the effectiveness. The effect of using different blade material can be seen when the FCE is averaged for the spacing distances between the holes. If the spacing between two consecutive holes is set to be $5D$ the drop in overall FCE is 6% for $K_R = 100$. However, at $K_R = 10000$ the drop in FCE is about

45%. Therefore, depending on the hole spacing and the safety factor for turbine operation, K_R can be used to set a higher limit for the range of materials that can be used in operating the turbine blade efficiently and economically.

It is clear from Figure 18 that using blades with higher thermal conductivity will reduce the overall FCE however; it will reduce temperature gradient with the blade material. Lower temperature gradient in desired to reduce thermal stresses within the blade nevertheless reducing the FCE is not desired. Hence, one needs to optimize the blade thermal conductivity based on maximum temperature allowed by the material and maximum allowed temperature gradient. This show that there is a room to improve the material selection, so it can stand high temperature and high temperature gradients.

Figure 20 shows how the temperature wall gradient varies for two thermal conductivity ratios. At $K_R = 1$, the coolant plenum experiences no heating from the mainstream gas, before and after the film cooling effect. However, at higher thermal conductivity ratio, $K_R = 10000$, the plenum wall temperature close to the film cooling hole is lower which increases the jet gas temperature, therefore reducing FCE.

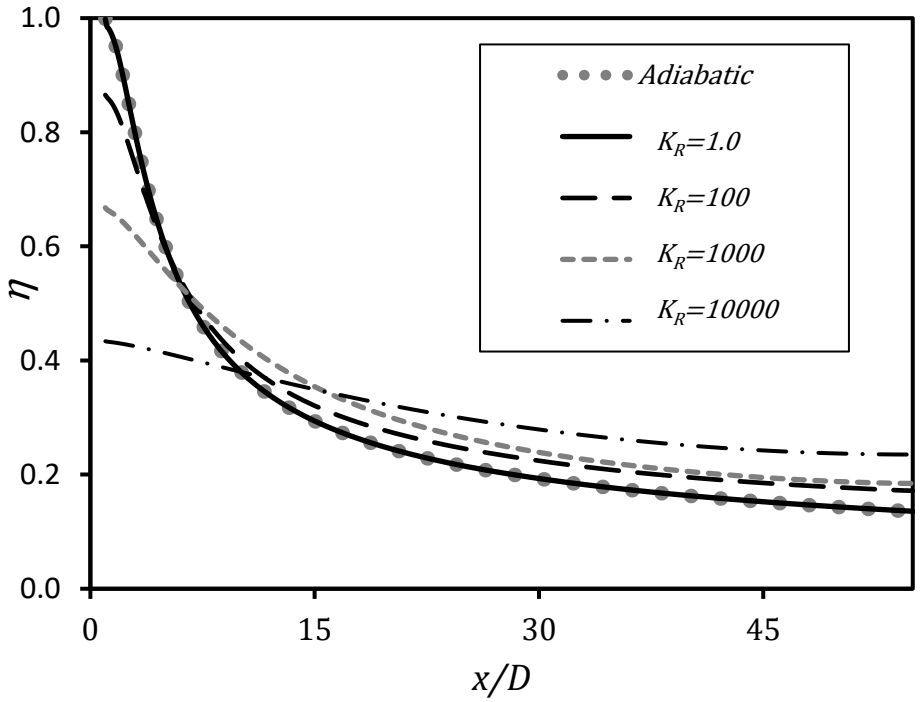

Figure 19: Conjugate heat transfer results for all K_R values

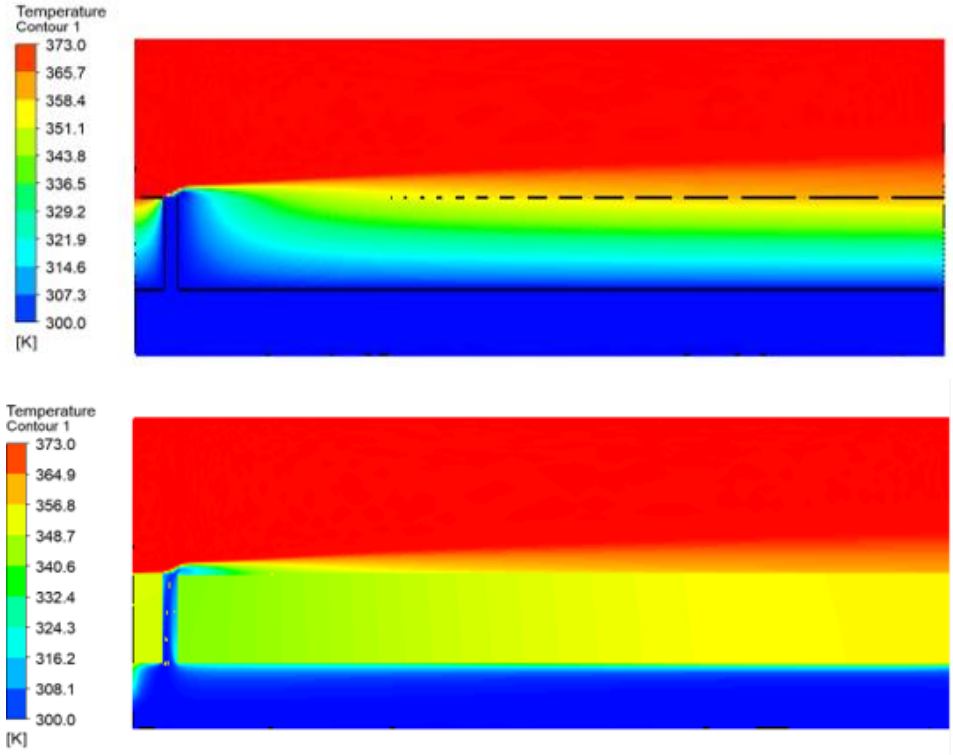

Figure 20: Temperature wall gradient. (a) $K_R = 1.0$ and (b) $K_R = 10000$

Chapter 5. Conclusion and Future Work

In this work, five main parameters effect on film cooling performance were discussed by using a 2D numerical model using ANSYS FLUENT. The five main parameters are blowing ratio, density ratio, injection angle, centrifugal force and blade material. The RNG $k-\varepsilon$ model with EWF is the selected turbulence model in this study as it captures the low-Reynolds number effects close to the wall. This turbulence model shows the best accuracy in reporting the AFCE compared to the other turbulence models.

Sensitivity analysis has shown that blowing ratio has the major effect on the AFCE. However, the most optimum parameter configuration is a combination of all affecting parameters. For the considered parameters configuration in the practical range for film cooling, the combination of injection angle of 30°, DR = 1.2 and M = 0.8 offers the highest average AFCE. Jet Reynolds number studies show the important role of film cooling blanket thickness in AFCE, bigger holes offer higher values of the film cooling blanket thickness. Centrifugal force alters the flow field and affects the film cooling blanket attachment to the turbine's blade surface causing the AFCE to fall sharply at high centrifugal accelerations which causes turbine blades to fail due to overheating at the blade tip. Finally, conjugate heat transfer analysis has shown the effect of thermal conductivity on FCE. Thermal conductivity ratios less than K_R=1 have shown almost no effect on FCE. However, higher ratios can eliminate film cooling effect on the turbine's blade surface.

The combined effects of centrifugal force, Coriolis effect and vortex formation on the FCE were not included. As a future work, a 3D model will be used to study the effect of the reported parameters on FCE including these effects. The effect of hole geometry, number of cooling holes, the spacing in lateral and span-wise direction has to be studied as well to have a full picture of all controlling parameters on FCE.

References

[1] Y. Çengel and M. Boles, *Thermodynamics: An Engineering Approach*, 8th Edition, New York: McGraw-Hill Education, 2015.

[2] D. Straub, T. Sidwell, K. Casleton, S. Chien and M. Chyu, "High Temperature Film Cooling Test Facility and Preliminary Test," in *Proceedings of ASME Turbo Expo 2012*, Copenhagen, 2012.

[3] M. Chyu and S. Siw, "Recent Advances of Internal Cooling Techniques for Gas Turbine Airfoils," *Journal of Thermal Science and Engineering Applications*, vol. 5, no. 2, 2013.

[4] R. Rezazadeh, M. Alizadeh, F. Alireza and H. Khaledi, "Turbine Blade Temperature Calculation and Life Estimation - A Sensitivity Analysis," *Propulsion and Power Research*, vol. 2, no. 2, pp. 148-161, 2013.

[5] B. Lakshminarayana, *Fluid Dynamics and Heat Transfer of Turbomachinery*, New York: Marcel Dekker, 1996.

[6] E. Elnajjar, M. Hamdan and Y. Haik, "Experimental Investigation of Internal Channel Cooling Via Jet Impingement," *FDMP: Fluid Dynamics & Materials Processing*, vol. 9, no. 1, pp. 77-89, 2013.

[7] M. Hamdan and A. Hayek, "Effect of Cavity Size on Confined Slot Jet Impingement Cooling," in *ASME 2013 Heat Transfer Summer Conference*, Minneapolis, 2013.

[8] M. Hamdan, E. Elnajjar and Y. Haik, "Measurement and Modeling of Confined Jet Discharged Tangentially on a Concave Semicylindrical Hot Surface," *Journal of Heat Transfer-transactions of The ASME*, vol. 133, no. 12, pp. 1222031-222037, 2011.

[9] M. Hamdan and M. Al-Nimr, "Thermal Augmentation in Internal Cooling Passage by Converting Impingement Jet to Induced Swirl Flow," in *6th International Conference on Computational Heat and Mass Transfer*, Guangzhou, 2009.

[10] E. Elnajjar, M. Hamdan and Y. Haik, "Experimental Investigation of Impinging Jet Flow on a Heated Curved Surface," in *6th International Conference on Thermal Engineering*, Istanbul, 2012.

[11] F. Bayley and A. Turner, "The Transpiration-Cooled Gas Turbine," *Journal of Engineering for Power*, vol. 92, no. 4, pp. 351-358, 1970.

[12] J. Wang, J. Messner and H. Stetter, "An Experimental Investigation of Transpiration Cooling. Part I: Application of an Infrared Measurement Technique," *International Journal of Rotating Machinery*, vol. 9, no. 3, pp. 153-161, 2003.

[13] D. Bogard and K. Thole, "Gas Turbine Film Cooling," *Journal of Propulsion and Power,* vol. 22, no. 2, 2005.

[14] R. Goldstein, "Film Cooling," *Advances in Heat Transfer,* vol. 7, pp. 321-379, 1971.

[15] B. Koff, "Gas Turbine Technology Overview - A Designer's Perspective," *AIAA/ICAS International Air and Space Symposium and Exposition: The Next 100 Years,* pp. 2003-2722, 2003.

[16] T. Pollock and S. Tin, "Nickel-Based Superalloys for Advanced Turbine Engines: Chemistry, Microstructure, and Properties," *Journal of Propulsion and Power,* vol. 22, no. 2, pp. 361-374, 2006.

[17] J. Nijo, J. Jayakumar and Y. Giridhara, "Numerical Investigation of Adiabatic Film Cooling Effectiveness over a Flat Plate Model With Cylindrical Holes," in *International Conference on Computational Heat and Mass Transfer,* 2015.

[18] T. Fric and A. Roshko, "Vortical Structure in The Wake of a Transverse Jet," *Journal of Fluid Mechanics,* vol. 279, no. 1, pp. 1-47, 1994.

[19] W. Plesniak and D. Cusano, "Scalar Mixing in a Confined Rectangular Jet in Crossflow," *Journal of Fluid Mechanics,* vol. 524, no. 1, pp. 1-45, 2005.

[20] C. Yuen and R. Martinez-Botas, "Film Cooling Characteristics of a Single Round Hole at Various Streamwise Angles in a Crossflow: Part I Effectiveness," *International Journal of Heat and Mass Transfer,* vol. 46, no. 2, pp. 221-235, 2003.

[21] J. Mayhew, J. Baughn and A. Byerley, "The Effect of Freestream Turbulence on Film Cooling Adiabatic Effectiveness," *International Journal of Heat and Fluid Flow,* vol. 24, no. 5, pp. 669-679, 2003.

[22] B. Mouzon, E. Terrell, J. Albert and D. Bogard, "Net Heat Flux Reduction and Overall Effectiveness for a Turbine Blade Leading Edge," in *ASME Turbo Expo 2005: Power for Land, Sea and Air*, Nevada, 2005.

[23] B. Johnson, W. Tian, K. Zhang and H. Hu, "An experimental study of density ratio effects on the film cooling injection from discrete holes by using PIV and PSP techniques," *International Journal of Heat and Mass Transfer,* vol. 76, no. 1, pp. 337-349, 2014.

[24] K. Singh, B. Premachandran and M. Ravi, "A Numerical Study on the 2D Film Cooling of a Flat Surface," *Numerical Heat Transfer,* vol. 67, no. 6, pp. 673-695, 2014.

[25] S. Bayraktar and T. Yilmaz, "Two-dimensional numerical investigation of film cooling by a cool jet injected at various angles for different blowing ratios," *J. Mechanical Engineering Science,* vol. 222, no. 12, pp. 1215-1224, 2008.

[26] C. Yuen and Martinez-Botas, "Film Cooling Characteristics of Rows of Round Holes at Various Streamwise Angles in a Crossflow: Part I Effectiveness,"

International Journal of Heat and Mass Transfer, vol. 48, no. 12-13, pp. 4995–5016, 2005.

[27] K. O'Malley, Theoritcal aspects of film cooling, PhD Thesis, University of Oxford, 1984.

[28] A. Mehendale and J. Han, "Reynolds Number Effect on Leading Edge Film Effectiveness And Heat Transfer Coefficient," *Heat Mass Transfer*, vol. 36, no. 15, pp. 3723-3730, 1993.

[29] S. Nasir, T. Bolchoz, W. Ng, L. Zhang, H. Moon and R. Anthony, "Showerhead Film Cooling Performance of a Turbine Vane at High Freestream Turbulence in a Transonic Cascade," *Journal of Turbomachinery*, vol. 134, no. 5, 2012.

[30] R. Jia, B. Sundén, P. Miron and B. Léger, "A Numerical and Experimental Investigation of the Slot Film-Cooling Jet With Various Angles," *Journal of Turbomachinery*, vol. 127, no. 3, pp. 635-645, 2005.

[31] R. Goldstein and E. Eckert, "Effects of Hole Geometry And Density on Three-Dimensional Film Cooling," *International Journal of Heat and Mass Transfer*, vol. 17, no. 5, pp. 595-607, 1974.

[32] K. Thole, M. Gritsch, A. Schulz and S. Wittig, "Flowfield Measurements for Film-Cooling Holes With Expanded Exits," *Journal of Turbomachinery*, vol. 120, no. 2, pp. 327-336, 1998.

[33] D. Schmidt, B. Sen and D. Bogard, "Film Cooling With Compound Angle Holes: Adiabatic Effectiveness," *Journal of Turbomachinery*, vol. 118, no. 4, pp. 807-813, 1996.

[34] P. Dai and F. Lin, "Numerical Study on Film Cooling Effectiveness From Shaped and Crescent Holes," *Heat and Mass Transfer*, vol. 47, no. 2, pp. 147-154, 2011.

[35] K. Kusterer, D. Bohn, T. Sugimoto and R. Tanaka, "Double-Jet Ejection of Cooling Air for Improved Film Cooling," *Journal of Turbomachinery*, vol. 129, no. 4, pp. 809-815, 2006.

[36] S. Baheri, S. Tabrizi and B. Jubran, "Film Cooling Effectiveness From Trenched Shaped and Compound Holes," *Heat and Mass Transfer*, vol. 44, no. 8, pp. 989-998, 2008.

[37] M. Ghorab and I. Hassan, "An Experimental Investigation of a New Hybrid Film Cooling Scheme," *International Journal of Heat and Mass Transfer*, vol. 53, no. 21-22, pp. 4994-5007, 2010.

[38] Y. Yao, J. Zhang and L. Wang, "Film Cooling on a Gas Turbine Blade Suction Side With Converging Slot-Hole," *International Journal of Thermal Sciences*, vol. 65, pp. 267-279, 2013.

[39] X. Zhu, L. Liu and F. Yuan, "Effect of Rotation on Flow Field and Film Cooling Effectiveness in Film-Cooled Turbine Rotors," *Int. J. Turbo Jet-Engines,* vol. 31, no. 4, pp. 361-370, 2014.

[40] N. Alzurfi, A. Turan, A. Nasser and A. Alhusseny, "Numerical Simulation of Film Cooling Effectiveness in a Rotating Blade at High Blowing Ratios," in *12th International Conference on Heat Transfer, Fluid Mechanics and Thermodynamic,* Costa de Sol, 2016.

[41] D. Rigby and J. Lepicovsky, "Conjugate Heat Transfer Analysis of Internally Cooled Configurations," in *ASME Turbo Expo 2001: Power for Land, Sea, and Air*, New Orleans, Louisiana, 2001.

[42] M. Silieti, E. Divo and A. Kassab, "The Effect of Conjugate Heat Transfer on Film Cooling Effectiveness," *International Journal of Computation and Methodology,* vol. 56, no. 5, pp. 335-350, 2010.

[43] J. Ferguson, D. Walters and J. Leylek, "Performance of Turbulence Models and Near-Wall Treatments in Discrete Jet Film Cooling Simulations," in *ASME 1998 International Gas Turbine and Aeroengine Congress and Exhibition*, Stockholm, 1998.

[44] W. York and J. Leylek, "Leading-Edge Film-Cooling Physics: Part I — Adiabatic Effectiveness," in *ASME Turbo Expo 2002: Power for Land, Sea, and Air*, Amsterdam, 2002.

[45] C. Nguyen, N. Tran, B. Bernier, S. Ho and J. Kapat, "Sensitivity Analysis for Film Effectiveness on a Round Film Hole Embedded in a Trench Using Conjugate Heat Transfer Numerical Model," in *ASME Turbo Expo 2010: Power for Land, Sea, and Air*, Glasgow, 2010.

[46] S. Turns, *Thermal Fluid Science-An Integral Approach*, Cambridge University Press, 2006.

[47] O. Oleĭnik and V. Samokhin, *Mathematical models in boundary layer theory*, Chapman & Hall, 1999.

[48] F. Menter, R. Langtry, S. Likki, Y. Suzen, P. Huang and S. Volker, "A Correlation-Based Transition Model Using Local Variables: Part I — Model Formulation," *Journal of Turbomachinery,* vol. 128, no. 3, pp. 413-422, 2014.

[49] D. C. Montgomery, *Introduction to Statistical Quality Control*, Hoboken: NJ: Wiley, 2013.

[50] "Power Engineering Internationl," 2012. [Online]. Available: http://www.powerengineeringint.com/content/dam/pei/print-articles/2012/april/gas-steam-tech.pdf. [Accessed 25 March 2018].

[51] S. Rani, A. K. Agrawal and V. Rastogi, "Failure Analysis of a First Stage IN738 gas Turbine Blade Tip Cracking in a Thermal Power Plant," *Case Studies in Engineering Failure Analysis,* vol. 8, no. 1, pp. 1-10, 2017.

Vita

Mohammed Aref Al-Hemyari was born in 1993, in Sana’a, Yemen. He received his primary and secondary education in Dubai, UAE. He received his B.Sc. degree in Renewable and Sustainable Engineering from the University of Sharjah in 2016.

In September 2016, he joined the Mechanical Engineering master's program in the American University of Sharjah as a graduate teaching assistant. During his master's study, he co-authored 2 papers which were presented in international conferences. His research interests are in renewable energy, thermal energy, fluid mechanics, heat transfer and CFD.